International Journal of Ambient Energy

ISSN: 0143-0750 (Print) 2162-8246 (Online) Journal homepage: www.tandfonline.com/journals/taen20

Non-similarity analysis of the magnetohydrodynamic flow of reactive Casson-Jeffrey nanofluids over a vertically stretching sheet with slip conditions

Hammed Abiodun Ogunseye, Yusuf Olatunji Tijani, Titilayo Morenike Agbaje, Shina Daniel Oloniiju & Olumuyiwa Otegbeye

To cite this article: Hammed Abiodun Ogunseye, Yusuf Olatunji Tijani, Titilayo Morenike Agbaje, Shina Daniel Oloniiju & Olumuyiwa Otegbeye (2025) Non-similarity analysis of the magnetohydrodynamic flow of reactive Casson-Jeffrey nanofluids over a vertically stretching sheet with slip conditions, International Journal of Ambient Energy, 46:1, 2557552, DOI: 10.1080/01430750.2025.2557552

To link to this article: https://doi.org/10.1080/01430750.2025.2557552

Published online: 26 Sep 2025.

INTERNATIONAL JOURNAL OF AMBIENT ENERGY
2025, VOL. 46, NO. 1, 2557552
https://doi.org/10.1080/01430750.2025.2557552

Taylor & Francis
Taylor & Francis Group

OPEN ACCESS Check for updates

Non-similarity analysis of the magnetohydrodynamic flow of reactive Casson-Jeffrey nanofluids over a vertically stretching sheet with slip conditions

Hammed Abiodun Ogunseye [a], Yusuf Olatunji Tijani [b], Titilayo Morenike Agbaje [c], Shina Daniel Oloniiju [b] and Olumuyiwa Otegbeye [c]

[a]West Virginia Academy, Al-Wukair, Doha, Qatar; [b]Department of Mathematics, Rhodes University, Grahamstown, South Africa; [c]School of Computer Science and Applied Mathematics, University of the Witwatersrand, Johannesburg, South Africa

ABSTRACT
The phenomenon of stretching sheets is vital in various industrial and engineering applications, significantly affecting the efficiency and quality of processes such as the manufacturing of electronic components, aerodynamic designs, among many others. This study explores the interaction between magnetohydrodynamics and a reactive viscous Casson-Jeffery nanofluid. The physical system is transformed into a mathematical framework by applying conservation laws and translating observable phenomena into precise, quantifiable equations. Non-similar analysis is used to transform the system into a dimensionless form. The system of differential equations is simplified into a linear form through the local linearization technique, after which a bivariate spectral-based method is implemented to approximate the solutions of the differential equations. The convergence analysis of the method confirms the reliability of the spectral-based technique. It was found that the Casson fluid has greater thermal sensitivity and higher fluid flow than the Jeffrey fluid. However, when the fluid parameters are varied, the Jeffrey fluid exhibits higher concentration peaks under identical conditions than the Casson fluid. The Jeffery fluid has higher species sensitivity than the Casson fluid. The findings of this study contribute to the understanding of complex fluid dynamics, which can be used to validate or refine theoretical models and simulations.

ARTICLE HISTORY
Received 16 October 2024
Accepted 29 August 2025

KEYWORDS
Casson fluid; Jeffrey fluid; spectral method; reactive nanofluid; differential equations

Nomenclature

(u, v)	Velocity components (m/s)
(x, y)	Cartesian coordinate (m)
M	magnetic field parameter, $\frac{\sigma_f B_0^2}{\rho_f U}$,
Gr_T	Grashof number due to temperature, $\frac{g\varepsilon_1(T_w-T_\infty)x^3}{\nu_f^2}$
Gr_C	Grashof number due to concentration, $\frac{g\varepsilon_2(C_w-C_\infty)x^3}{\nu_f^2}$
λ_2	thermal buoyancy parameter, $\frac{Gr_T}{Re^2}$
Re	local Reynolds number, $\frac{Ux}{\nu_f}$
λ_3	concentration buoyancy parameter, $\frac{Gr_C}{Re^2}$
De	dimensionless Deborah number, $\frac{\lambda_1 U}{x}$,
f_w	suction parameter, $V\left(\frac{x}{\nu_f U}\right)^{\frac{1}{2}}$
δ_1	velocity slip parameter $N_0\left(\frac{U}{x\nu_f}\right)^{\frac{1}{2}}$,
δ_2	temperature slip parameter $K_0\left(\frac{U}{x\nu_f}\right)^{\frac{1}{2}}$
ν	kinematic viscosity (m^2/s)
μ	dynamic viscosity $(kgm^{-1}s^{-1})$
f	base fluid
A	constant
β	Casson fluid parameter
U	the velocity at the vertical plate
σ	electrical conductivity (S/m)
Pr	Prandtl number, $\frac{(\mu c_p)_f}{k_f}$
B	variable magnetic field
Ec	Eckert number, $\frac{U2}{(cp)f(T-T\infty)}$
ρ	density (kg/m^3)
N_r	thermal radiation parameter, $\frac{16\sigma^* T_\infty^3}{3\kappa k_f}$
g	gravitational acceleration (m/s^2)
Nb	Brownian movement parameter, $\frac{(\rho c_p)_p D_B(C_w-C_\infty)}{(\rho c_p)_f \nu_f}$
T	fluid temperature (K)
N_t	thermophoresis parameter, $\frac{(\rho c_p)_p D_B(T_w-T_\infty)}{(\rho c_p)_f \nu_f T_\infty}$
C	concentration (kg/m^3)
Le	Lewis number, $\frac{\nu_f}{D_B}$
k_f	thermal conductivity (Wm^{-1}K^{-1})
Kr	chemical reaction parameter, $\frac{k_r^2 x}{U}$
cp	specific heat capacity (J/kgK)
E	non-dimensional activation energy, $\frac{E_a}{\kappa T_\infty}$
D_B	Brownian diffusion coefficient
Cf	skin friction coefficient
D_T	coefficient of thermophoresis diffusion
Nu	local Nusselt number
Q	non-uniform heat source/sink (W/m^3)
Sh	local Sherwood number
kr	reaction rate (1/s)
j	mass flux
E_a	activation energy (J/mol)
λ	ratio of relaxation to retardation times

CONTACT Yusuf Olatunji Tijani olodyusuf@gmail.com

n	fitted rate constant
λ_1	retardation time
T_w	wall temperature
B_0	uniform magnetic field (A/m)
ϵ_1	coefficient of thermal expansion (K^{-1})
ϵ_2	coefficient of concentration expansion (m^3/kg)
σ_*	Stefan–Boltzmann constant
κ_*	mean absorption coefficient (m^{-1})
κ	Boltzmann constant
Ω	temperature ratio, $\Omega = \frac{T_w}{T_\infty}$
η, ξ	similarity variables
θ	normalised temperature
ϕ	normalised concentration
∞	in the ambient condition
w	conditions on the wall
τ	shear stress

1. Introduction

Fluid flow played a critical role in the fourth industrial revolution (4IR), which was characterised by the integration of digital technologies, artificial intelligence, and advanced materials into various industries. The fluid mechanics principles underpin many technological advancements driving this revolution and have far-reaching implications for manufacturing, energy, transportation, and healthcare industries (Schwab 2016). Advances in HVAC (heating, ventilation, and air conditioning) systems leverage fluid mechanics to improve air distribution and energy efficiency in buildings (Kusiak, Li, and Tang 2010). Microfluidic devices rely on an understanding of fluid flow to control and manipulate fluids at microscopic scales. This technology is used in lab-on-a-chip devices for diagnostics and chemical analysis, enabling faster and more accurate testing (Neuzil et al. 2012). In the healthcare and industrial environments, many fluids with significant applications fall into non-Newtonian fluids, which, unlike Newtonian fluids, exhibit variable viscosity that changes with shear rate or applied stresse (Kundu, Cohen, and Dowling 2016; White 2006). This behaviour makes non-Newtonian fluids particularly useful in a variety of practical applications. Among the many constitutive models of non-Newtonian fluids, Casson and Jeffrey fluids are particularly notable due to their distinct shear-dependent viscosity, yield stress, and time-dependent characteristics (Das, Mahato, and Nandkeolyar 2015; Wajihah and Sankar 2023). The constitutive relation of the Casson fluid is given by Siddiqui, Farooq, and Rana (2015)

$$\sqrt{\tau} = \sqrt{\tau_d} + \sqrt{\xi\dot{\Phi}}, \rightarrow \tau = [(\tau_d\xi)^{0.5}|\dot{\Phi}|^{-0.5} + \xi]\dot{\Phi} + \mathcal{O}(|\dot{\Phi}|^2), \tag{1}$$

where τ, τ_d, ξ and $\dot{\Phi}$ represent the shear strain, Casson yield stress, Casson viscosity and shear rate, respectively. On the other hand, the constitutive equation of the Jeffery fluid is expressed as (Qasim 2013)

$$\mathbf{Y_d} = -p\mathbf{I} + \frac{\mu}{1+\lambda_1}\left[\left(\frac{\partial\Psi_1}{\partial t} + (\mathbf{V}\cdot\nabla)\Psi_1\right)\lambda_1 + \Psi_1\right], \tag{2}$$

here, $\mathbf{Y_d}$ is the stress tensor, p is the pressure, $\mathbf{I}$ is the identity tensor, μ is the dynamic viscosity, $\mathbf{V}$ stands for the velocity vector, Ψ_1 is the first Rivlin-Ericksen tensor, λ_1 and λ_2 are material constants representing the relaxation and retardation times, respectively.

The Casson and Jeffery fluid models have been a subject of research interest due to their practical importance and industrial relevance (Khan et al. 2021; Mahesh, Mahabaleshwar, and Sofos 2023). Tijani et al. (2024b) analysed the rotational effects and the influence of a nanofluid on the flow of a Jeffery fluid over an expanding surface. The impact of internal heat generation, magnetic field strength, and thermal radiation on the flow of a Jeffery fluid over an expanding surface was studied by Dadhich et al. (2021). Ullah et al. (2024) analysed the flow of Jeffery fluid within a stretching cylinder using a non-parabolic heat transfer model. Their study provided insights into the thermal behaviour of the fluid, emphasising the complex interaction between the stretching motion and nonlinear heat transfer effects. The study of Akolade, Adeosun, and Olabode (2021) offers critical insights into how thermophysical properties influence the MHD squeezed flow of dissipative Casson fluid. The analysis deepens our understanding of fluid dynamics in complex industrial processes by including the effects of chemical reactions and radiation.

In the studies above, the governing deterministic models were transformed into a dimensionless form using a technique known as dimensional analysis. Dimensional analysis is a powerful tool used in scientific studies to simplify mathematical models (by reducing the number of variables) and understand the fundamental relationships between them. It can broadly be categorised into two approaches: similarity analysis and non-similarity analysis (White 2006). The analysis of transport phenomena in boundary layer flows has long been dominated by the use of similarity transformations. This mathematical technique is celebrated for its elegance and effectiveness in reducing a system of non-linear partial differential equations (PDEs) into a more tractable system of non-linear ordinary differential equations (ODEs). Non-similarity analysis focuses on finding dimensionless groups and the dimensional relationships among the variables so that no dimensionless parameters are expressed as a function of the state or time variables (White 2006). This approach often leads directly to transforming the dimensional differential equation into dimensionless differential equations. Sparrow, Quack, and Boerner (1970) demonstrated that boundary layer problems exhibiting non-similarity analysis characteristics arise in many scenarios. These include dynamical models with variations in wall temperature, free-stream conditions, and buoyancy forces, among many others. Lawal et al. (2023) applied the local non-similarity technique to convert a partial differential equation modelling the boundary layer flow over a stretching flat plate into a dimensionless, single-variable differential equation. Tijani et al. (2024a) applied a non-similarity technique to study the behaviour of a magnetic dipole in the flow of a Reiner-Philipoff fluid over an expanding surface. Jan, Mushtaq, and Hussain (2024) systematically reduced the conservation equations into dimensionless deterministic form through a non-similar group of transformations. The local non-similarity method reduces the dimensionless PDEs to ordinary differential equations. Additional research in this area can be found in the studies conducted by Hamid, Khan, and Hussain (2020), Shukla et al. (2022). In other related studies, (Haider, Gul, and

Nadeem 2023) analysed the heat transport and peristaltic flow through an asymmetric channel having variable viscosity and electric conductivity. The analysis revealed the critical role of temperature-dependent properties in the peristaltic transport of nanofluids. An increase in viscosity, which acts as an internal resistance to flow, leads to a significant decrease in both the volumetric flow rate and the pressure gradient. Conversely, an enhancement in electrical conductivity promotes thermal activity, resulting in a higher fluid temperature and a corresponding increase in the heat transfer rate. Ashraf et al. (2024) investigated the forced convection effect for heat transport in a rectangular channel with obstacles using the finite element method. The results include the implications of the rarefaction effect on fluid flow and heat transmission, and decisions regarding the location of barriers and the shape of obstacles in squares. Mkhatshwa (2024) investigates the quadratic convective flow of a nanofluid over an inclined porous plate, incorporating variable fluid properties, chemical reactions, and activation energy. The governing equations are solved using a multi-domain spectral collocation method. Results show that while plate inclination improves thermal performance, it reduces flow velocity. Variable viscosity and nonlinear convection enhance both flow speed and heat transfer. Notably, activation energy boosts nanoparticle concentration but suppresses the mass transfer rate. For further study, we refer to Mkhatshwa, Motsa, and Sibanda (2022) and Tijani (2025). It is generally observed that many researchers prefer using similarity transformations over non-similarity techniques, as similarity transformations tend to reduce the dynamic conservation equations to ordinary differential equations (Minkowycz and Cheng 1982). Non-similar transformations, on the other hand, often result in partial differential equations. Ordinary differential equations are easier to resolve with readily available numerical and semi-analytic methods. Handling partial differential equations with multiple variables is inherently complex, and few numerical methods can efficiently resolve such systems. However, the non-similar transformation should be applied when appropriate for scientific accuracy and correctness (Pantokratoras 2019). Numerical methods such as Chebyshev spectral methods have been developed and implemented to address the challenges associated with finding solutions to such complex problems (Magagula et al. 2016; Motsa and Animasaun 2016). The properties of the Chebyshev spectral method are well established (Trefethen 2000), and various studies have effectively combined linearisation approaches with spectral methods to address highly nonlinear problems (Goqo et al. 2018; Magagula, Motsa, and Sibanda 2020; RamReddy and Rao 2017). One such approach is the bivariate spectral local linearisation method (BSLLM) (Motsa 2015). Several studies have applied the BSLLM (Makanda and Shaw 2019; Sithole et al. 2019), demonstrating its high efficiency, ease of implementation, and computational cost-effectiveness. These properties underscore the importance of conducting this current investigation using the BSLLM. Standard time-stepping methods like the Runge–Kutta scheme (RK4), the finite difference scheme would require very small step-sizes to maintain stability and accuracy for this highly non-linear dynamical model. BSLLM, by treating the problem globally in both variables, avoids this time-stepping limitation and can be more efficient for finding solutions over a large domain. The local linearisation approach in BSLLM results in a sequence of simpler, structured linear problems that are more computationally efficient to solve at each iteration.

Considering studies in the literature, to the authors' knowledge, no study has adequately investigated the reactive MHD Casson-Jeffery fluid in a vertically stretching sheet. This study examines the boundary layer flow of a Casson-Jeffery fluid on a continuously moving slip sheet with Arrhenius-type reaction, heat source/sink, and nonlinear thermal radiation. The remainder of this study is organised into four sections. Section 2 focuses on translating the physical model into a mathematical model. Section 3 describes the bivariate spectral-based method used to approximate the solution of the dynamical system. Section 4 presents the interpretation and analysis of the solution profiles. Finally, Section 5 concludes the study.

2. Model formulation

This study investigates the behaviour of the mixed convective flow of an incompressible Casson-Jeffrey nanofluid (CJNF) flowing steadily towards a vertically stretching plate. We focus on how heat and mass transfer are influenced when the temperature and concentration at the plate's surface exceed those in the surrounding fluid. A variable magnetic field, $B(x) = B_0 x^{-\frac{1}{2}}$ is applied perpendicularly to the flow direction, where B_0. is a constant magnetic fld strength. We use Buongiorno's model to describe the effects of thermophoresis and Brownian motion on the CJNF flow; see Figure 1. Additionally, several variables affecting heat transfer are considered, including viscous dissipation, nonlinear thermal radiation, Joule heating, and the influence of a heat sink or source. The analysis also examines how Arrhenius activation energy and binary chemical processes impact mass transfer. The conservation equations for mass, momentum, temperature, and concentration in the CJNF flow, upon incorporating the assumptions mentioned above, are expressed as follows (see [Sandeep and Sulochana 2018], and [Khan et al. 2017]):

$$\frac{\partial u}{\partial x} + \frac{\partial v}{\partial y} = 0, \tag{3}$$

$$\begin{aligned} u\frac{\partial u}{\partial x} + v\frac{\partial u}{\partial y} &= \frac{\nu_f}{1+\lambda}\left[\left(1+\frac{1}{\beta}\right)\left(\frac{\partial^2 u}{\partial y^2}\right)\right. \\ &\quad \left. + \lambda_1\left(\frac{\partial u}{\partial y}\frac{\partial^2 u}{\partial x \partial y} + u\frac{\partial^3 u}{\partial x \partial y^2} - \frac{\partial u}{\partial x}\frac{\partial^2 u}{\partial y^2} + v\frac{\partial^3 u}{\partial y^3}\right)\right] \\ &\quad - \frac{\sigma_f B(x)^2}{\rho_f}u + g(\varepsilon_1(T-T_\infty) + \varepsilon_2(C-C_\infty)), \end{aligned} \tag{4}$$

$$\begin{aligned} u\frac{\partial T}{\partial x} + v\frac{\partial T}{\partial y} &= \frac{k_f}{(\rho c_p)_f}\left(\frac{\partial^2 T}{\partial y^2}\right) + \frac{1}{(\rho c_p)_f}\frac{16\sigma^*}{3\kappa^*}\frac{\partial}{\partial y}\left(T^3\frac{\partial T}{\partial y}\right) \\ &\quad + \frac{(\rho c_p)_p}{(\rho c_p)_f}\left(D_B\frac{\partial C}{\partial y}\frac{\partial T}{\partial y} + \frac{D_T}{T_\infty}\left(\frac{\partial T}{\partial y}\right)^2\right) \\ &\quad + \frac{\mu_f}{(\rho c_p)_f(1+\lambda)}\left[\left(1+\frac{1}{\beta}\right)\frac{\partial^2 u}{\partial y^2}\right. \\ &\quad \left. + \lambda_1\left(u\frac{\partial u}{\partial y}\frac{\partial^2 u}{\partial x \partial y} + v\frac{\partial u}{\partial y}\frac{\partial^2 u}{\partial y^2}\right)\right] \end{aligned}$$

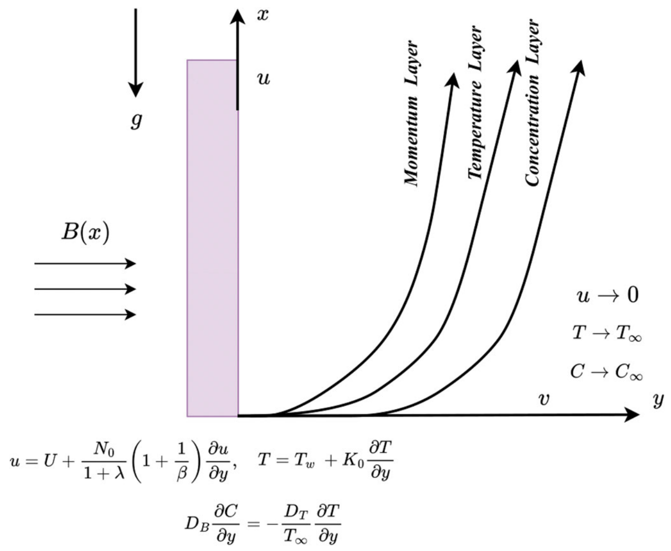

Figure 1. Physical outlook of the mathematical model.

$$+\frac{\sigma_f B_0^2}{(\rho c_p)_f}u^2 + \frac{Q^*}{(\rho c_p)_f}, \tag{5}$$

$$u\frac{\partial C}{\partial x} + v\frac{\partial C}{\partial y} = D_B\frac{\partial^2 C}{\partial y^2} + \frac{D_T}{T_\infty}\frac{\partial^2 T}{\partial y^2} - k_r^2(C - C_\infty)\left(\frac{T}{T_\infty}\right)^n \exp\left(\frac{-E_a}{\kappa T}\right). \tag{6}$$

The conditions associated with the flow are similar to those considered in Kuznetsov and Nield (2014), Mukhopadhyay (2013), Turkyilmazoglu (2016), and are defined as follows:

$$\left.\begin{aligned}
&u = U + \frac{N_0}{1+\lambda}\left(1+\frac{1}{\beta}\right)\frac{\partial u}{\partial y},\ v = -V,\ T = T_w + K_0\frac{\partial T}{\partial y},\\
&D_B\frac{\partial C}{\partial y} + \frac{D_T}{T_\infty}\frac{\partial T}{\partial y} = 0 \text{ at } y = 0,\\
&u \to 0,\ T \to T_\infty,\ C \to C_\infty \text{ as } y \to \infty.
\end{aligned}\right\} \tag{7}$$

It is important to mention that the conditions given in Equation (7) replace the standard 'no-slip' assumptions with more realistic slip effects for both velocity and temperature at the surface. Furthermore, the model assumes zero net nanoparticle flux at the wall, where the tendency of particles to move via Brownian motion is counteracted by thermophoresis, i.e. $\frac{\partial C}{\partial y}|_{y=0} + \frac{D_T}{T_\infty}\frac{\partial T}{\partial y}|_{y=0}$. The far-field conditions ensure the fluid returns to its ambient state. The non-constant heat source Q^* follows the definition given in (Sandeep and Sulochana 2018)

$$Q^* = \frac{k_f U_w(T_w - T_\infty)}{x\nu_f}\left(\gamma_1\frac{\partial f}{\partial \eta} + \gamma_2\frac{T - T_\infty}{T_w - T_\infty}\right), \tag{8}$$

where $\gamma_1, \gamma_2 \in (0, \infty)$ indicates the scenario of heat generation, whereas the case of heat absorption is given as $\gamma_1, \gamma_2 \in (-\infty, 0)$. The system of Equations (3)–(6) is reduced to a coupled system of nonlinear ordinary differential equations by introducing the following group of similarity transformations (see [Patil, Roy, and Chamkha 2010])

$$\left.\begin{aligned}
&\xi(x) = \left(\frac{Ux}{\nu_f}\right)^{\frac{1}{2}},\ \eta(x,y) = y\left(\frac{U}{\nu_f x}\right)^{\frac{1}{2}},\\
&\psi(x,y) = (\nu_f x U)^{\frac{1}{2}} f(\eta,\xi),\\
&\theta(\eta,\xi) = \frac{T - T_\infty}{T_w - T_\infty},\ \phi(\eta,\xi) = \frac{C - C_\infty}{C_w - C_\infty},
\end{aligned}\right\} \tag{9}$$

where ψ is the stream function such that $(u,v) \equiv (\partial\psi/\partial y, -\partial\psi/\partial x)$ and satisfies the continuity Equation (3). Upon substituting Equations (8) and (9) into Equations (4) to (7), the conservation equations and boundary conditions become:

$$\begin{aligned}
&\left(1+\frac{1}{\beta}\right)\frac{\partial^3 f}{\partial \eta^3} + (1+\lambda)\left(\frac{1}{2}f\frac{\partial^2 f}{\partial \eta^2} - M\frac{\partial f}{\partial \eta} + \lambda_2\theta + \lambda_3\phi\right)\\
&-\frac{De}{2}\left(\left(\frac{\partial^2 f}{\partial \eta^2}\right)^2 + f\frac{\partial^4 f}{\partial \eta^4} + 2\frac{\partial f}{\partial \eta}\frac{\partial^3 f}{\partial \eta^3}\right)\\
&+\frac{(1+\lambda)\xi}{2}\left(\frac{\partial f}{\partial \xi}\frac{\partial^2 f}{\partial \eta^2} - \frac{\partial f}{\partial \eta}\frac{\partial^2 f}{\partial \xi\partial \eta}\right)\\
&+\frac{De\xi}{2}\left(\frac{\partial^2 f}{\partial \eta^2}\frac{\partial^3 f}{\partial \xi\partial \eta^2} + \frac{\partial f}{\partial \eta}\frac{\partial^4 f}{\partial \xi\partial \eta^3} - \frac{\partial^3 f}{\partial \eta^3}\frac{\partial^2 f}{\partial \xi\partial \eta} - \frac{\partial f}{\partial \xi}\frac{\partial^4 f}{\partial \eta^4}\right) = 0,
\end{aligned} \tag{10}$$

$$\begin{aligned}
&\frac{1}{Pr}\frac{\partial}{\partial \eta}\left(1 + Nr((\Omega-1)\theta+1)^3\frac{\partial \theta}{\partial \eta}\right) + \frac{1}{2}f\frac{\partial \theta}{\partial \eta} - \frac{\partial f}{\partial \eta}\theta\\
&+MEc\left(\frac{\partial f}{\partial \eta}\right)^2 + \left(Nb\frac{\partial \theta}{\partial \eta}\frac{\partial \phi}{\partial \eta} + Nt\left(\frac{\partial \theta}{\partial \eta}\right)^2\right)\\
&+\gamma_1\frac{\partial f}{\partial \eta} + \gamma_2\theta + \frac{Ec}{(1+\lambda)}\left(1+\frac{1}{\beta}\right)\left(\frac{\partial^2 f}{\partial \eta^2}\right)^2\\
&-\frac{EcDe}{2(1+\lambda)}\left(f\frac{\partial^2 f}{\partial \eta^2}\frac{\partial^3 f}{\partial \eta^3} + \frac{\partial f}{\partial \eta}\left(\frac{\partial^2 f}{\partial \eta^2}\right)^2\right)\\
&+\frac{\xi}{2}\left(\frac{\partial f}{\partial \xi}\frac{\partial \theta}{\partial \eta} - \frac{\partial f}{\partial \eta}\frac{\partial \theta}{\partial \xi}\right) + \frac{EcDe\xi}{2(1+\lambda)}\\
&\times\left(\frac{\partial f}{\partial \eta}\frac{\partial^2 f}{\partial \eta^2}\frac{\partial^3 f}{\partial \xi\partial \eta^2} - \frac{\partial^2 f}{\partial \eta^2}\frac{\partial^3 f}{\partial \eta^3}\frac{\partial f}{\partial \xi}\right) = 0,
\end{aligned} \tag{11}$$

$$\begin{aligned}
&\frac{1}{Le}\frac{\partial^2 \phi}{\partial \eta^2} + \frac{1}{2}f\frac{\partial \phi}{\partial \eta} + \frac{1}{Le}\frac{Nt}{Nb}\frac{\partial^2 \theta}{\partial \eta^2} + K_r((\Omega-1)\theta+1)^n\phi\\
&\times\exp\left(\frac{-E}{(\Omega-1)\theta+1}\right) + \frac{\xi}{2}\left(\frac{\partial f}{\partial \xi}\frac{\partial \phi}{\partial \eta} - \frac{\partial f}{\partial \eta}\frac{\partial \phi}{\partial \xi}\right) = 0,
\end{aligned} \tag{12}$$

and

$$\left.\begin{aligned}
&f(0,\xi) + \xi\left.\frac{\partial f}{\partial \xi}\right|_{\eta=0} = f_w,\ f'(0,\xi) = 1\\
&+\left(1+\frac{1}{\beta}\right)\delta_1 f''(0,\xi),\ f'(\infty,\xi) \to 0,\\
&\theta(0,\xi) = 1 + \delta_2\theta'(0,\xi),\ \theta(\infty,\xi) \to 0,\\
&Nb\phi'(0,\xi) + Nt\theta'(0,\xi) = 0,\ \phi(\infty,\xi) \to 0,
\end{aligned}\right\} \tag{13}$$

where $'$ denotes the partial differentiation with respect to η. The skin friction, Nusselt number, and Sherwood number are, respectively, defined as

$$Cf = \frac{2\tau_w}{\rho_f U^2},\ Nu = \frac{xq_w}{k_f(T_w - T_\infty)},\ \text{and } Sh = \frac{xj_w}{D_B(C_w - C_\infty)}, \quad (14)$$

where the wall shear stress τ_w, the wall flux q_w, and the wall mass flux are expressed as:

$$\left.\begin{aligned} \tau_w &= \frac{\mu_f}{1+\lambda}\left(\left(1+\frac{1}{\beta}\right)\left(\frac{\partial u}{\partial y}\right)\right. \\ &+ \left.\left.\lambda_1\left(u\frac{\partial^2 u}{\partial x\partial y} + v\frac{\partial^2 u}{\partial y^2}\right)\right)\right|_{y=0}, \\ q_w &= -\left(k_f + \frac{16\sigma^* T^3}{3\kappa^*}\right)\left.\frac{\partial T}{\partial y}\right|_{y=0},\ j_w = -D_b\left.\frac{\partial C}{\partial y}\right|_{y=0}. \end{aligned}\right\} \quad (15)$$

The dimensionless form of Equation (14) takes the form

$$\begin{aligned} Re^{\frac{1}{2}}Cf &= \frac{1}{1+\lambda}\left[2\left(1+\frac{1}{\beta}\right)\frac{\partial^2 f(\eta,\xi)}{\partial\eta^2}\right. \\ &\quad \left. - Def(\eta,\xi)\frac{\partial^3 f(\eta,\xi)}{\partial\eta^3}\right]_{\eta=0}, \\ Re^{-\frac{1}{2}}Nu &= -(1 + Nr((\Omega-1)\theta(0,\xi)+1)^3)\theta'(0,\xi), \\ Re^{-\frac{1}{2}}Sh &= -\phi'(0,\xi). \end{aligned} \quad (16)$$

3. Numerical procedure

Equations (10)–(12) are solved subject to the corresponding boundary conditions in Equation (13) using the bivariate spectral local linearisation method (BSLLM). The BSLLM is a numerical method that uses first-order Taylor series expansion to linearise nonlinear equations in a system (Motsa 2013). The Taylor series expansion effectively leads to the decoupling of the original system and ensures that updated solutions to equations are immediately used in subsequent equations. The resulting linear decoupled system of equations is integrated using the Chebyshev spectral collocation method that uses bivariate Lagrange interpolation polynomials as basis functions. Applying the Taylor series expansion to Equations (10)–(12) result in the following system of decoupled linear partial differential equations:

$$\left.\begin{aligned} & a_{0,r}f_{r+1}'''' + a_{1,r}f_{r+1}''' + a_{2,r}f_{r+1}'' + a_{3,r}f_{r+1}' + a_{4,r}f_{r+1} \\ & + a_{5,r}\frac{\partial f'''_{r+1}}{\partial\xi} + a_{6,r}\frac{\partial f''_{r+1}}{\partial\xi} + \\ & a_{7,r}\frac{\partial f'_{r+1}}{\partial\xi} + a_{8,r}\frac{\partial f_{r+1}}{\partial\xi} = R_{1,r}, \\ & b_{0,r}\theta_{r+1}'' + b_{1,r}\theta_{r+1}' + b_{2,r}\theta_{r+1} + b_{3,r}\frac{\partial\theta_{r+1}}{\partial\xi} = R_{2,r}, \\ & c_{0,r}\phi_{r+1}'' + c_{1,r}\phi_{r+1}' + c_{2,r}\phi_{r+1} + c_{3,r}\frac{\partial\phi_{r+1}}{\partial\xi} = R_{3,r}, \end{aligned}\right\} \quad (17)$$

where

$$\left.\begin{aligned} a_{0,r} &= -\frac{De}{2}f_r - \frac{De}{2}\xi\frac{\partial f_r}{\partial\xi}, \\ a_{1,r} &= \left(1+\frac{1}{\beta}\right) - \frac{De}{2}2f_r' - \frac{De}{2}\xi\frac{\partial f'_r}{\partial\xi}, \\ a_{2,r} &= \frac{1}{2}f_r(1+\lambda) - \frac{De}{2}2f_r'' \\ &+ \frac{(1+\lambda)}{2}\xi\frac{\partial f_r}{\partial\xi} + \frac{De}{2}\xi\frac{\partial f''_r}{\partial\xi}, \\ a_{3,r} &= -M(1+\lambda) - \frac{De}{2}2f_r''' \\ &+ \frac{(1+\lambda)}{2}\xi\frac{\partial f'_r}{\partial\xi} + \frac{De}{2}\xi\frac{\partial f'''_r}{\partial\xi}, \\ a_{4,r} &= (1+\lambda)\frac{1}{2}f_r'' - \frac{De}{2}f_r'''', \\ a_{5,r} &= \frac{De}{2}\xi f_r',\ a_{6,r} = \frac{De}{2}\xi f_r'', \\ a_{7,r} &= -\frac{(1+\lambda)}{2}\xi f_r' - \frac{De}{2}\xi f_r''', \\ a_{8,r} &= \frac{(1+\lambda)}{2}\xi f_r' - \frac{De}{2}\xi f_r'''', \\ b_{0,r} &= \frac{Nr}{Pr}[(\Omega-1)\theta_r+1]^3, \\ b_{1,r} &= \frac{6Nr}{Pr}[(\Omega-1)\theta_r+1]^2(\Omega-1)\theta_r \\ &+ \frac{1}{2}f_{r+1} + Nb\phi_r' + 2Nt\theta_r' + \frac{1}{2}\xi\frac{\partial f_{r+1}}{\partial\xi}, \\ b_{2,r} &= \frac{6Nr}{Pr}[(\Omega-1)\theta_r+1](\Omega-1)^2\theta_r'^2 \\ &+ \frac{3Nr}{Pr}(\Omega-1)[(\Omega-1)\theta_r+1]^2 \\ & \theta_r'' - f_{r+1}' + \gamma_2, \\ b_{3,r} &= -\frac{1}{2}\xi f_{r+1}', \\ c_{0,r} &= \frac{1}{Le},\ c_{1,r} = \frac{1}{2}f_{r+1} + \frac{1}{2}\xi\frac{\partial f_{r+1}}{\partial\xi}, \\ c_{2,r} &= Kr[(\Omega-1)\theta_{r+1}+1]^n \\ & \exp\left[\frac{-E}{(\Omega-1)\theta_{r+1}+1}\right], \\ c_{3,r} &= -\frac{1}{2}f_{r+1}'. \end{aligned}\right\} \quad (18)$$

The right hand side of Equation (17) are defined as:

$$\left.\begin{aligned} R_{1,r} &= a_{0,r}f_r'''' + a_{1,r}f_r''' + a_{2,r}f_r'' + a_{3,r}f_r' + a_{4,r}f_r \\ &+ a_{5,r}\frac{\partial f'''_r}{\partial\xi} + a_{6,r}\frac{\partial f''_r}{\partial\xi} + a_{7,r}\frac{\partial f'_r}{\partial\xi} + a_{8,r}\frac{\partial f_r}{\partial\xi} - H_1, \\ R_{2,r} &= b_{0,r}\theta_r'' + b_{1,r}\theta_r' + b_{2,r}\theta_r + b_{3,r}\frac{\partial\theta_r}{\partial\xi} + b_{4,r}f_r''' \\ &+ b_{5,r}f_r'' + b_{6,r}f_r' + b_{7,r}f_r''' + \\ &\quad b_{8,r}\frac{\partial f''_r}{\partial\xi} + b_{9,r}\frac{\partial f_r}{\partial\xi} + b_{10,r}\phi_r' - H_2, \\ R_{3,r} &= c_{0,r}\phi_r'' + c_{1,r}\phi_r' + c_{2,r}\phi_r + c_{3,r}\frac{\partial\phi_r}{\partial\xi} + c_{4,r}f_r' \\ &+ c_{5,r}f_r + c_{6,r}\frac{\partial f_r}{\partial\xi} + c_{7,r}\theta_r'' + c_{8,r}\theta_r - H_3, \end{aligned}\right\} \quad (19)$$

and $H_m (m = 1, 2, 3)$ are defined as:

$$\left.\begin{aligned}
H_1 &= \left(1+\frac{1}{\beta}\right) f_r''' + (1+\lambda)\left[\frac{1}{2} f_r f_r'' - M f_r' + \lambda_2 \theta_r + \lambda_3 \phi_r\right] \\
&- \frac{De}{2}[f_r''^2 + f_r f_r'''' + 2 f_r' f_r'''] + \frac{(1+\lambda)}{2}\xi\left[f_r''\frac{\partial f_r}{\partial \xi} - f_r'\frac{\partial f_r'}{\partial \xi}\right] \\
&+ \frac{De}{2}\xi\left[f_r''\frac{\partial f_r''}{\partial \xi} + f_r'\frac{\partial f_r'''}{\partial \xi} - f_r'''\frac{\partial f_r'}{\partial \xi} - f_r''''\frac{\partial f_r}{\partial \xi}\right], \\
H_2 &= \frac{3Nr}{Pr}[(\Omega-1)\theta_r + 1]^2 \theta_r'^2 (\Omega - 1) \\
&+ \frac{Nr}{Pr}[(\Omega-1)\theta_r + 1]^3 \theta_r'' + \frac{1}{2} f_{r+1}\theta_r' - f_{r+1}'\theta_r - MEcf_{r+1}'^2 \\
&\quad + Nb\theta_r'\phi_r' + Nt\theta_r'^2 + \gamma_1 f_{r+1}' + \gamma_2 \theta_r \\
&+ \frac{Ec}{1+\lambda}\left(1+\frac{1}{\beta}\right) f_{r+1}''^2 - \frac{EcDe}{2(1+\lambda)} \\
&[f_{r+1} f_{r+1}'' f_{r+1}''' + f_{r+1}' f_{r+1}''^2] + \frac{1}{2}\xi\left[\frac{\partial f_{r+1}}{\partial \xi}\theta_r' - f_{r+1}'\frac{\partial \theta_r}{\partial \xi}\right] \\
&+ \frac{EcDe}{2(1+\lambda)}\xi\left[f_{r+1}' f_{r+1}''\frac{\partial f_{r+1}''}{\partial \xi} - f_{r+1}'' f_{r+1}'''\frac{\partial f_{r+1}}{\partial \xi}\right], \\
H_3 &= \frac{1}{Le}\phi_r'' + \frac{1}{2} f_r \phi_r' + \frac{1}{Le}\frac{Nt}{Nb}\theta_{r+1}'' \\
&+ Kr[(\Omega-1)\theta_{r+1} + 1]^n \phi_r \\
&\exp\left[\frac{-E}{(\Omega-1)\theta_{r+1}+1}\right] + \frac{1}{2}\xi\left[\phi_r'\frac{\partial f_{r+1}}{\partial \xi} - f_{r+1}'\frac{\partial \phi_r}{\partial \xi}\right].
\end{aligned}\right\} \tag{20}$$

To apply the spectral collocation method in both the η and ξ dimensions, the physical domains $\xi \in [0, 1]$ and $\eta \in [0, L_\infty]$ are converted to the computational domain $[-1, 1]$, and the Chebyshev Gauss-Lobatto nodes are used for collocation. The nodes are defined in (Trefethen 2000) and (Canuto et al. 2006) as;

$$\eta_i = \cos\left(\frac{\pi i}{N_\eta}\right), \ \xi_j = \cos\left(\frac{\pi j}{N_\xi}\right), \ i = 0, 1, \cdots N_\eta,$$
$$j = 0, 1, \cdots, N_\xi, \ \eta \in [-1, 1], \ \xi \in [-1, 1]. \tag{21}$$

It is convenient to write

$$\left.\begin{aligned}
&\left.\frac{\partial^n f}{\partial \eta^n}\right|_{(\xi_j,\eta_i)} = \mathbf{D}^n \mathbf{F}_j, \quad \left.\frac{\partial^n \theta}{\partial \eta^n}\right|_{(\xi_j,\eta_i)} = \mathbf{D}^n \Theta_j, \quad \left.\frac{\partial^n \phi}{\partial \eta^n}\right|_{(\xi_j,\eta_i)} = \mathbf{D}^n \Phi_j, \\
&\left.\frac{\partial f}{\partial \xi}\right|_{(\xi_j,\eta_i)} = \sum_{q=0}^{N_\xi} \mathbf{d}_{jq}\mathbf{F}_q, \quad \left.\frac{\partial \theta}{\partial \xi}\right|_{(\xi_j,\eta_i)} = \sum_{q=0}^{N_\xi} \mathbf{d}_{jq}\Theta_q, \quad \left.\frac{\partial \phi}{\partial \xi}\right|_{(\xi_j,\eta_i)} \\
&= \sum_{q=0}^{N_\xi} \mathbf{d}_{jq}\Phi_q,
\end{aligned}\right\} \tag{22}$$

where $i = 0, 1, \cdots, N_\eta$, $\mathbf{d}_{jq}$ are entries of the standard first-order Chebyshev differentiation matrix of size $(N_\xi + 1)$ by $(N_\xi + 1)$ in ξ dimension, $\mathbf{D}^n$ is the standard nth-order Chebyshev differentiation matrix of size $(N_\eta + 1)$ by $(N_\eta + 1)$. These differentiation matrices are scaled accordingly as $\mathbf{d} = 2\mathbf{d}$ and $\mathbf{D} = \frac{2}{L_\infty}\mathbf{D}$, where $\mathbf{d}$ is the differentiation matrix associated with the variable ξ, $\mathbf{D}$ is the differentiation matrix associated with the variable η, L_∞ is a number large enough to represent the truncation of the semi-infinite domain at infinity. The solutions of Equation (17) are assumed to be approximated in terms of the bivariate Lagrange interpolation polynomials of the form:

$$\left.\begin{aligned}
f(\eta,\xi) &\approx \sum_{p=0}^{N_\eta} \sum_{q=0}^{N_\xi} f(\eta_p,\xi_q) L_p(\eta) L_q(\xi), \\
\theta(\eta,\xi) &\approx \sum_{p=0}^{N_\eta} \sum_{q=0}^{N_\xi} \theta(\eta_p,\xi_q) L_p(\eta) L_q(\xi), \\
\phi(\eta,\xi) &\approx \sum_{p=0}^{N_\eta} \sum_{q=0}^{N_\xi} \phi(\eta_p,\xi_q) L_p(\eta) L_q(\xi),
\end{aligned}\right\} \tag{23}$$

where the functions $L_p(\eta)$ and $L_q(\xi)$ are the characteristic Lagrange cardinal polynomials, defined as:

$$L_p(\eta) = \prod_{\substack{i=0 \\ i \neq p}}^{N_\eta} \frac{\eta - \eta_i}{\eta_p - \eta_i}, L_q(\xi) = \prod_{\substack{j=0 \\ j \neq q}}^{N_\xi} \frac{\xi - \xi_j}{\xi_q - \xi_j}, \tag{24}$$

with the following properties

$$L_p(\eta_i) = \delta_{ip} = \begin{cases} 0 \text{ if } i \neq p \\ 1 \text{ if } i = p, \end{cases} \quad L_q(\xi_j) = \delta_{jq} = \begin{cases} 0 \text{ if } j \neq q \\ 1 \text{ if } j = q. \end{cases} \tag{24}$$

The vectors $\mathbf{F}_j$, Θ_j and Φ_j in Equation (21) are the vectors of solutions $f(\eta), \theta(\eta)$ and $\phi(\eta)$ at each ξ_j-level, and are defined, respectively, as

$$\left.\begin{aligned}
\mathbf{F}_j &= [f(\eta_0,\xi_j), f(\eta_1,\xi_j), \ldots, f(\eta_{N_\eta},\xi_j)]^T, \\
\Theta_j &= [\theta(\eta_0,\xi_j), \theta(\eta_1,\xi_j), \ldots, \theta(\eta_{N_\eta},\xi_j)]^T, \\
\Phi_j &= [\phi(\eta_0,\xi_j), \phi(\eta_1,\xi_j), \ldots, \phi(\eta_{N_\eta},\xi_j)]^T,
\end{aligned}\right\} \tag{25}$$

and the superscript T denotes a matrix transpose. Substituting Equation (22) into Equation (17) gives:

$$\begin{aligned}
&[\mathbf{a}_{0,r}\mathbf{D}^4 + \mathbf{a}_{1,r}\mathbf{D}^3 + \mathbf{a}_{2,r}\mathbf{D}^2 + \mathbf{a}_{3,r}\mathbf{D} + \mathbf{a}_{4,r}\mathbf{I} + \mathbf{a}_{5,r}\mathbf{d}_{jj}(\mathbf{D}^3) \\
&\quad + \mathbf{a}_{6,r}\mathbf{d}_{jj}(\mathbf{D}^2) + \mathbf{a}_{7,r}\mathbf{d}_{jj}(\mathbf{D}) + \mathbf{a}_{8,r}\mathbf{d}_{jj}\mathbf{I}] \\
&\mathbf{F}_{j,r+1} + \sum_{\substack{q=0 \\ j \neq q}}^{N_\xi} [\mathbf{a}_{5,r}\mathbf{d}_{jq}(\mathbf{D}^3) + \mathbf{a}_{6,r}\mathbf{d}_{jq}(\mathbf{D}^2) + \mathbf{a}_{7,r}\mathbf{d}_{jq}(\mathbf{D}) \\
&\quad + \mathbf{a}_{8,r}\mathbf{d}_{jq}\mathbf{I}]\mathbf{F}_{q,r+1} = R_{1,j,r}.
\end{aligned} \tag{26}$$

$$[\mathbf{b}_{0,r}\mathbf{D}^2 + \mathbf{b}_{1,r}\mathbf{D} + \mathbf{b}_{2,r}\mathbf{I} + \mathbf{b}_{3,r}\mathbf{d}_{jj}\mathbf{I}]\Theta_{j,r+1} + \sum_{\substack{q=0 \\ j \neq q}}^{N_\xi} [\mathbf{b}_{3,r}\mathbf{d}_{jq}\mathbf{I}]\Theta_{q,r+1}, = R_{2,j,r}, \tag{27}$$

$$[\mathbf{c}_{0,r}\mathbf{D}^2 + \mathbf{c}_{1,r}\mathbf{D} + \mathbf{c}_{2,r}\mathbf{I} + \mathbf{c}_{3,r}\mathbf{d}_{jj}\mathbf{I}]\Phi_{j,r+1} + \sum_{\substack{q=0 \\ j \neq q}}^{N_\xi} [\mathbf{c}_{3,r}\mathbf{d}_{jq}\mathbf{I}]\Phi_{q,r+1} = R_{3,j,r}, \tag{28}$$

where $\mathbf{I}$ is an identity matrix of size $(N_\eta + 1)$ by $(N_\eta + 1)$ and bold variable coefficients, $\mathbf{a}_{:,r}, \mathbf{b}_{:,r}, \mathbf{c}_{:,r}$, represent the diagonalisation of the corresponding vectors, where each vector is positioned along the diagonal of a matrix, with zeros elsewhere. In matrix-vector form, Equations (26)–(28) are, respectively, expressed as;

$$\mathbf{A}_1\mathbf{F} = \begin{bmatrix} A11_{0,0} & A11_{0,1} & \cdots & A11_{0,N_\xi} \\ A11_{1,0} & A11_{1,1} & \cdots & A11_{1,N_\xi} \\ \vdots & \vdots & \ddots & \vdots \\ A11_{N_\xi,0} & A11_{N_\xi,1} & \cdots & A11_{N_\xi,N_\xi} \end{bmatrix} \begin{bmatrix} \mathbf{F}_{0,r+1} \\ \mathbf{F}_{1,r+1} \\ \vdots \\ \mathbf{F}_{N_\xi,r+1} \end{bmatrix} = \begin{bmatrix} R_{0,1,r+1} \\ R_{1,1,r+1} \\ \vdots \\ R_{1,N_\xi,r+1} \end{bmatrix} = \mathbf{R}_1, \tag{29a}$$

$$\mathbf{A}_2\Theta = \begin{bmatrix} A22_{0,0} & A22_{0,1} & \cdots & A22_{0,N_\xi} \\ A22_{1,0} & A22_{1,1} & \cdots & A22_{1,N_\xi} \\ \vdots & \vdots & \ddots & \vdots \\ A22_{N_\xi,0} & A22_{N_\xi,1} & \cdots & A22_{N_\xi,N_\xi} \end{bmatrix} \begin{bmatrix} \Theta_{0,r+1} \\ \Theta_{1,r+1} \\ \vdots \\ \Theta_{N_\xi,r+1} \end{bmatrix} = \begin{bmatrix} R_{2,0,r} \\ R_{2,1,r+1} \\ \vdots \\ R_{2,N_\xi,r+1} \end{bmatrix} = \mathbf{R}_2, \tag{29b}$$

$$\mathbf{A}_3\Phi = \begin{bmatrix} A33_{0,0} & A33_{0,1} & \cdots & A33_{0,N_\xi} \\ A33_{1,0} & A33_{1,1} & \cdots & A33_{1,N_\xi} \\ \vdots & \vdots & \ddots & \vdots \\ A33_{N_\xi,0} & A33_{N_\xi,1} & \cdots & A33_{N_\xi,N_\xi} \end{bmatrix} \begin{bmatrix} \Phi_{0,r+1} \\ \Phi_{1,r+1} \\ \vdots \\ \Phi_{N_\xi,r+1} \end{bmatrix} = \begin{bmatrix} R_{3,0,r} \\ R_{3,1,r+1} \\ \vdots \\ R_{3,N_\xi,r+1} \end{bmatrix} = \mathbf{R}_3, \tag{29c}$$

where

$$\left.\begin{aligned} &A11_{j,j} = \mathbf{a}_{0,r}\mathbf{D}^4 + \mathbf{a}_{1,r}\mathbf{D}^3 + \mathbf{a}_{2,r}\mathbf{D}^2 + \mathbf{a}_{3,r}\mathbf{D} + \mathbf{a}_{4,r}\mathbf{I} \\ &+ \mathbf{a}_{5,r}\mathbf{d}_{jj}(\mathbf{D}^3) + \mathbf{a}_{6,r}\mathbf{d}_{jj}(\mathbf{D}^2) + \mathbf{a}_{7,r}\mathbf{d}_{jj}(\mathbf{D}) + \mathbf{a}_{8,r}\mathbf{d}_{jj}\mathbf{I}, \\ &A22_{j,j} = \mathbf{b}_{0,r}\mathbf{D}^2 + \mathbf{b}_{1,r}\mathbf{D} + \mathbf{b}_{2,r}\mathbf{I} + \mathbf{b}_{3,r}\mathbf{d}_{jj}\mathbf{I}, \;\; A33_{j,j} = \mathbf{c}_{0,r}\mathbf{D}^2 \\ &+ \mathbf{c}_{1,r}\mathbf{D} + \mathbf{c}_{2,r}\mathbf{I} + \mathbf{c}_{3,r}\mathbf{d}_{jj}\mathbf{I}, \\ &A11_{j,q} = \mathbf{a}_{5,r}\mathbf{d}_{jq}(\mathbf{D}^3) + \mathbf{a}_{6,r}\mathbf{d}_{jq}(\mathbf{D}^2) + \mathbf{a}_{7,r}\mathbf{d}_{jq}(\mathbf{D}) + \mathbf{a}_{8,r}\mathbf{d}_{jq}\mathbf{I}, \\ &A22_{j,q} = \mathbf{b}_{3,r}\mathbf{d}_{jq}\mathbf{I}, \;\; A33_{j,q} = \mathbf{c}_{3,r}\mathbf{d}_{jq}\mathbf{I}, \;\; j \neq q. \end{aligned}\right\} \tag{30}$$

Equation (29) is solved sequentially subject to appropriate initial guesses, which are functions that satisfy the boundary conditions (13). To this end, the following functions are chosen as the initial guesses

$$F_0(\eta) = f_w + \frac{1}{1 + \left(1 + \frac{1}{\beta}\right)\delta_1} - \frac{1}{1 + \left(1 + \frac{1}{\beta}\right)\delta_1} e^{-\eta},$$

$$\Theta_0(\eta) = \frac{1}{1 + \delta_2} e^{-\eta}, \;\; \Phi_0(\eta) = \frac{Nb}{Nt(1 + \delta_2)} e^{-\eta}. \tag{31}$$

We also note that A_1, A_2, and A_3 are matrices of size $N_\xi(N_\eta + 1) \times N_\xi(N_\eta + 1)$ and $A11$, $A22$, and $A33$ are matrices of size $(N_\eta + 1) \times (N_\eta + 1)$. We also remark that the boundary conditions given by Equation (13) are imposed on the matrices $A11_{j,j}$, $A22_{j,j}$, and $A33_{j,j}$ while the corresponding rows of the off-diagonal matrices $A22_{j,q}$ and $A33_{j,q}$ are imposed with zeros, except $A11_{j,q}$ that has $-\xi d_{N_\eta,q}$ imposed on the last row and zeros on rows 1 and $N_\eta - 1$.

3.1. Convergence analysis

In this section, convergence analysis is conducted to demonstrate that after a certain number of iterations, the solution of the partial differential Equations (10)–(12) solved subject to the boundary conditions in Equation (13) converges to a particular numerical value.

Table 1 shows that by the 25th iteration, the variables $-f''(0,\xi)$, $-\theta'(0,\xi)$ and $-\phi'(0,\xi)$ for both the Casson and Jeffery fluid cases converge to stable numerical values, indicating the accuracy and stability of the computational method employed in reaching a solution. Thus, the spectral-based method used in this study can be considered effective in providing satisfactory solutions to the system of differential equations under study. For the sake of completeness, Figure 2 is presented to reaffirm the convergence of the method using the engineering parameters. The parametric values are the same as those in Table 1, except for $Pr = 8.0$, $Ec = 0.3$, $M = 1.0$, $f_w = 1.0$, and $\Omega = 1.0$. We note that after a few iterations, the numerical values of the wall drag, wall heat and mass transfer coefficients remain constant.

4. Results and discussion

This section discusses the computational results obtained using the bivariate spectral-based method outlined in Section 3. To start with, Figure 3 shows the sparsity patterns of the matrices on the left-hand side of Equation (29), which is of size $((N_\eta + 1) \cdot (N_\xi + 1))$ by $((N_\eta + 1) \cdot (N_\xi + 1))$. In this case, $N_\eta = 100$ and $N_\xi = 10$, so the matrices are of size 1111 by 1111. Unless specified otherwise, $\beta = 1.2$, $De = 0.01$, $\lambda = 0.1$, and the default parameter values used for the numerical simulation are listed in Table 2.

It is vital to highlight that this study investigates the behaviour of two incompressible fluids, the Casson and the Jeffery fluids, simultaneously flowing over an expanding surface with slip conditions. Specifically, the Casson fluid model is recovered by setting the Jeffery parameter, $\lambda = 0$, and the Deborah number, $De = 0$. It is also noteworthy that while the Deborah number is not a primary parameter for the Jeffery fluid, it arises from the non-similar analysis due to the constitutive relation of the Jeffery fluid. The Jeffery fluid model is obtained by taking the limit of the Casson parameter, $\beta \to \infty$. The effect of the magnetic parameter is illustrated in Figure 4. Examining the conservation equations describing the flow reveals that the magnetic force acts as a resistive force in the momentum equation while serving as a supportive force in the energy equation. This

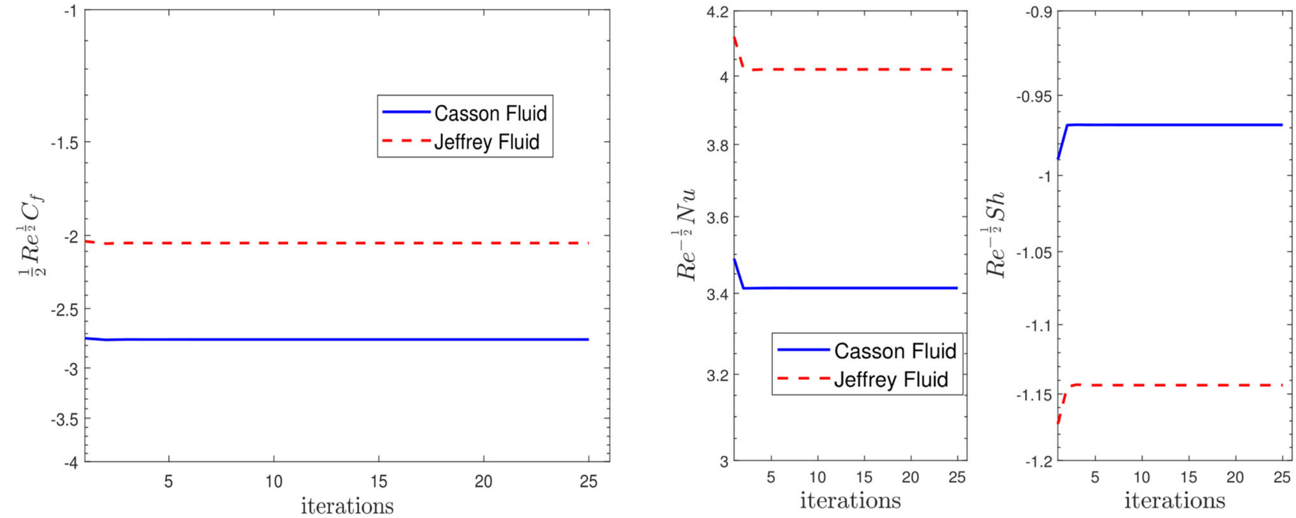

Figure 2. Convergence of the engineering parameters.

Table 1. Convergence of the BSLLM solution when $f_w = 0.8$, $Nr = 0.5$, $\lambda_2 = 0.2$, $\lambda_3 = 0.2$, $\delta_1 = 0.1, M = 2.0$, $\Omega = 1.0$, $Pr = 7.2$, $Ec = 0.5$, $Nt = 0.15$, $\gamma_2 = 0.1$, $\gamma_2 = 0.1$, $\delta = 0.1$, $\delta_2 = 0.02$, $Kr = 0.05$, $E = 0.2$, $Nb = 0.2$, $n = 1.0$ and $\xi = 1.0$.

	Casson ($\beta = 1.2$, $\lambda = 0.0$, $De = 0.0$)				Jeffrey ($\beta \to \infty$, $\lambda = 0.2$, $De = 0.01$)			
Variables	Iteration				Iteration			
	5	10	24	25	5	10	24	25
$-f''(0,\xi)$	0.9306546	0.9304906	0.9304907	0.9304907	1.4845719	1.4843595	1.4843595	1.4843595
$-\theta'(0,\xi)$	0.4492491	0.4490364	0.4490368	0.4490368	1.3758664	1.3785872	1.3785794	1.3785796
$\phi'(0,\xi)$	0.3369368	0.3367773	0.3367776	0.3367776	1.0318998	1.0339404	1.0339346	1.0339346

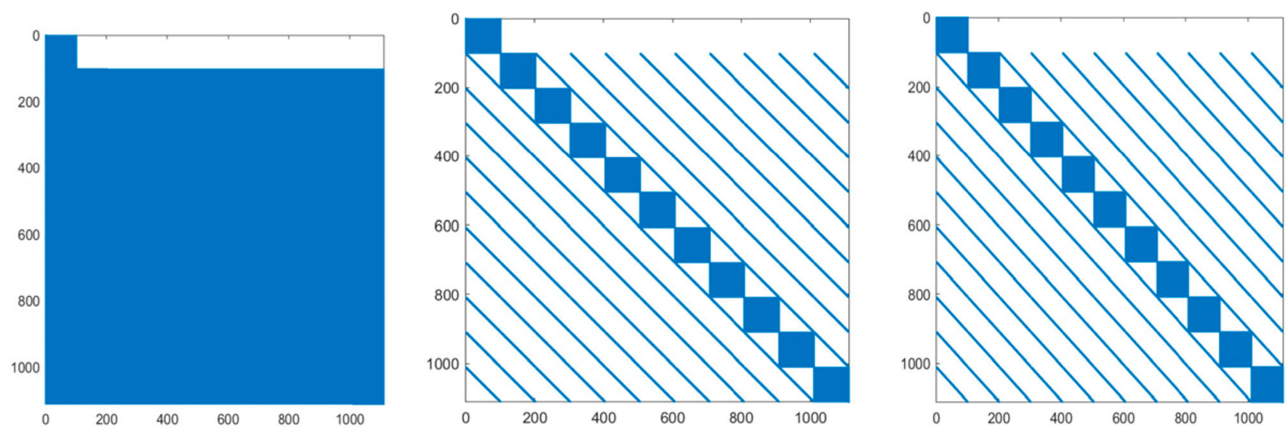

Figure 3. The sparsity patterns of the matrices on the left-hand side of Equation (29), left: matrix $\mathbf{A}_1$; middle: matrix $\mathbf{A}_2$; and right: matrix $\mathbf{A}_3$.

Table 2. Parameter values used for the numerical simulation.

Parameter	Value	Parameter	Value	Parameter	Value	Parameter	Value	Parameter	Value	Parameter	Value
f_w	0.8	N_r	0.5	λ_2	0.2	λ_3	0.2	δ_1	0.1	Pr	7.2
Ec	0.5	Nb	0.2	N_t	0.15	γ_2	0.1	γ_1	0.1	δ	0.1
δ_2	0.02	ω	1.0	Le	1.5	Kr	0.05	E	0.2	n	1.0

dual role is consistent for the Casson and the Jeffrey fluids flowing over the stretching surface. As the magnetic field becomes more substantial, the Lorentz force generated acts against the flow direction, leading to a decrease in the velocity of the fluids. Consequently, the increased magnetic resistance restricts the motion of the fluids, resulting in reduced flow rates. Thus, while the magnetic field provides some stabilising effects, it simultaneously impedes the fluid's ability to flow freely, particularly under the influence of a stretching surface. For the temperature profile , there is a transition in the behaviour of the fluids subject to a variation in the magnetic field parameter. Interestingly, this slower flow allows particles or solutes within the fluid more time to diffuse and accumulate, leading to higher concentration levels. This improved mixing helps distribute solutes more evenly and facilitates a higher concentration distribution.

Figure 5 shows the impact of the temperature ratio on the fluids' profiles. Temperature ratio (Ω) represents the ratio of the actual temperature difference to a reference or characteristic

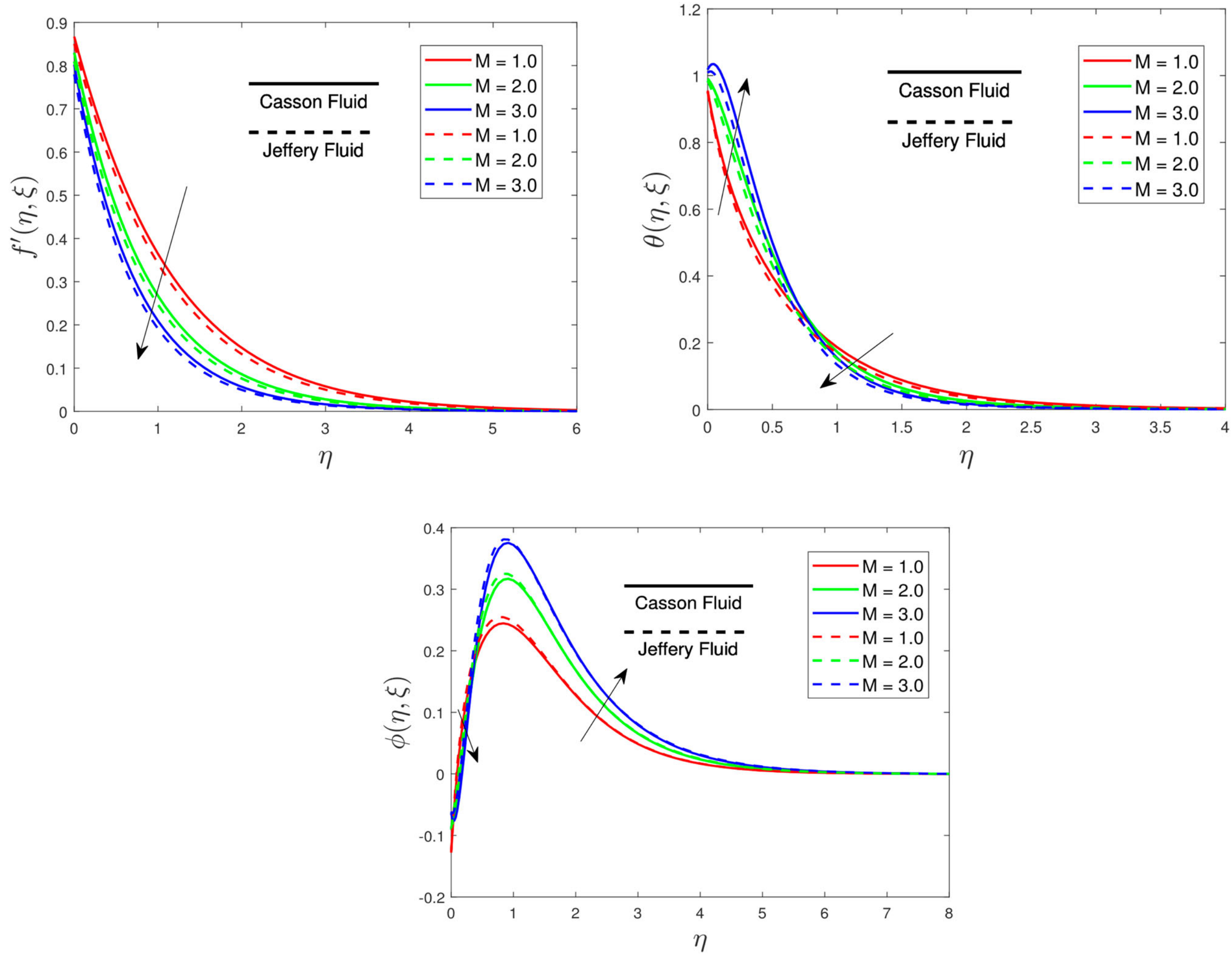

Figure 4. Magnetic (M) influence on the flow profiles.

temperature. As Ω increases, the curves seem to shift slightly. For Casson and Jeffery fluids, an increase in Ω appears to reduce the magnitude of the velocity gradient near the surface ($\eta = 0$). This result suggests that higher Ω values lead to decreased momentum change due to reduced fluid heating or internal friction. The parameter Ω affects the temperature distribution in the boundary layer. Higher values of Ω enhance the thermal boundary layer of both fluids. For the Casson fluid, the temperature drop is steeper than the Jeffery fluid, which suggests higher sensitivity to thermal variations. The Jeffery fluid shows a more gradual decrease in temperature, implying that it retains heat over a longer distance compared to the Casson fluid. As Ω increases, the concentration profile of both fluids exhibits a noticeable peak before satisfying the boundary layer condition. This dynamics indicates that the concentrations of the fluids reach a maximum for some physical parameters (e.g. heat flux, thermal conductivity) at a particular distance from the surface.

Figure 6 shows the impact of the activation energy and Lewis parameters on the concentration profiles of the fluids. Activation energy (E) is related to the minimum energy required for a chemical reaction to occur in the fluid. In the context of fluid flow, it is also associated with the rate at which a concentration gradient is affected by a reaction or diffusion process. For the two fluids, the concentration profiles exhibit a peak near $\eta = 1$ and then decay as the surface is stretched. As E increases, the concentration peaks drop and shift slightly to the right. The physical meaning here is that the concentration buildup near the surface is higher; however, diffusion into the fluid slows down, leading to a slower decay in concentration as the fluids move away from the wall. Lewis number (Le) is the thermal and mass diffusivity ratio. It measures the relative rate of heat transfer to mass transfer in a system. The enhancement in (Le) shows thermal diffusion dominates over mass diffusion, leading to a lower peak concentration and a more gradual decay for both fluids. The Casson fluid shows more sensitivity to changes in (Le), while the Jeffery fluid experiences smoother changes in concentration profiles. Brownian motion parameter (Nb) induced kinetic disturbances in the particles of both fluids.

As shown in Figure 7, Casson fluid exhibits greater thermal sensitivity and tendency to flow compared to Jeffrey fluid, except for species distribution. Boosting the Brownian parameter in this scenario increases the fluids' viscosities, thus reducing the fluids' flow rates. The heat and concentration also decrease because more reactants are used. Thermophoresis refers to the movement of microscopic particles driven by temperature differences within the surrounding medium. Figure 8 confirms that the thermophoresis parameter Nt exhibits a behaviour opposite to that of the Brownian motion parameter for the flow profiles.

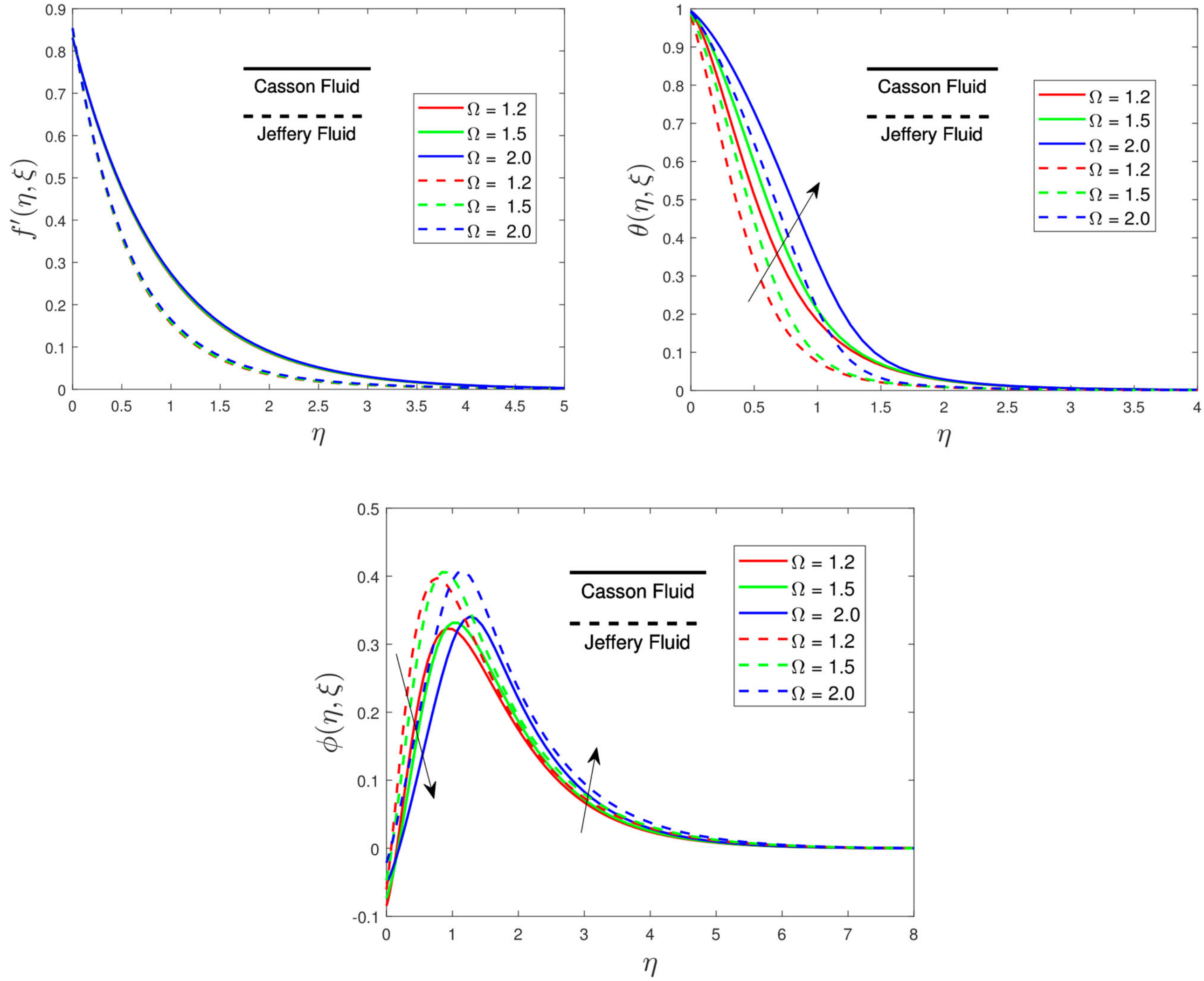

Figure 5. Temperature ratio (Ω) influence on the flow profiles.

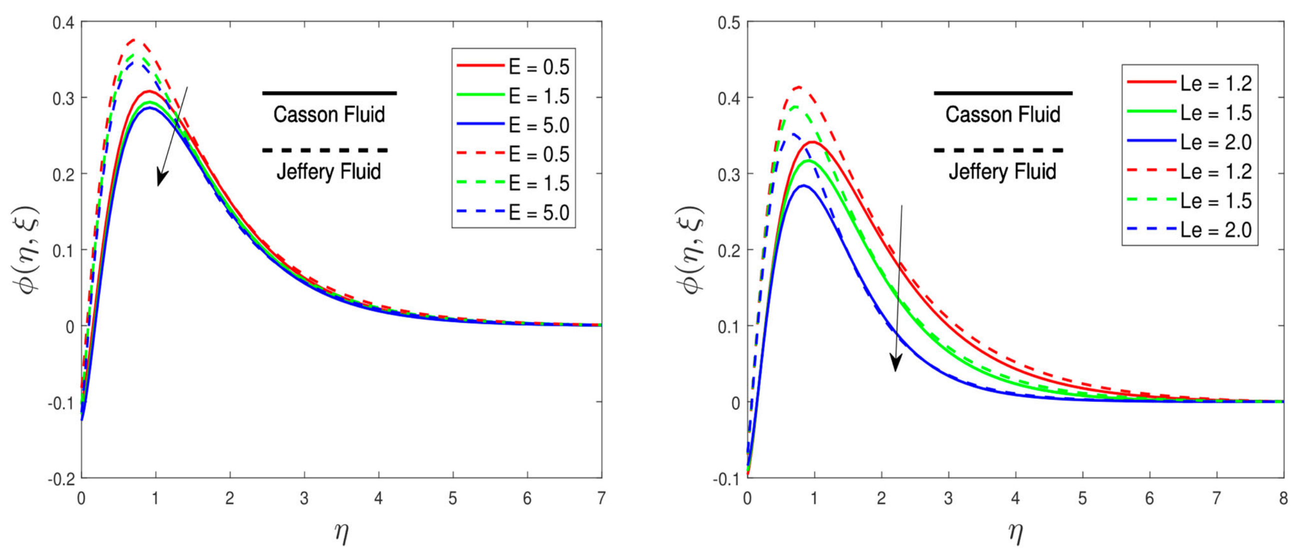

Figure 6. Activation parameter (E) and Lewis fluid parameter (Le) influence on the concentration profile.

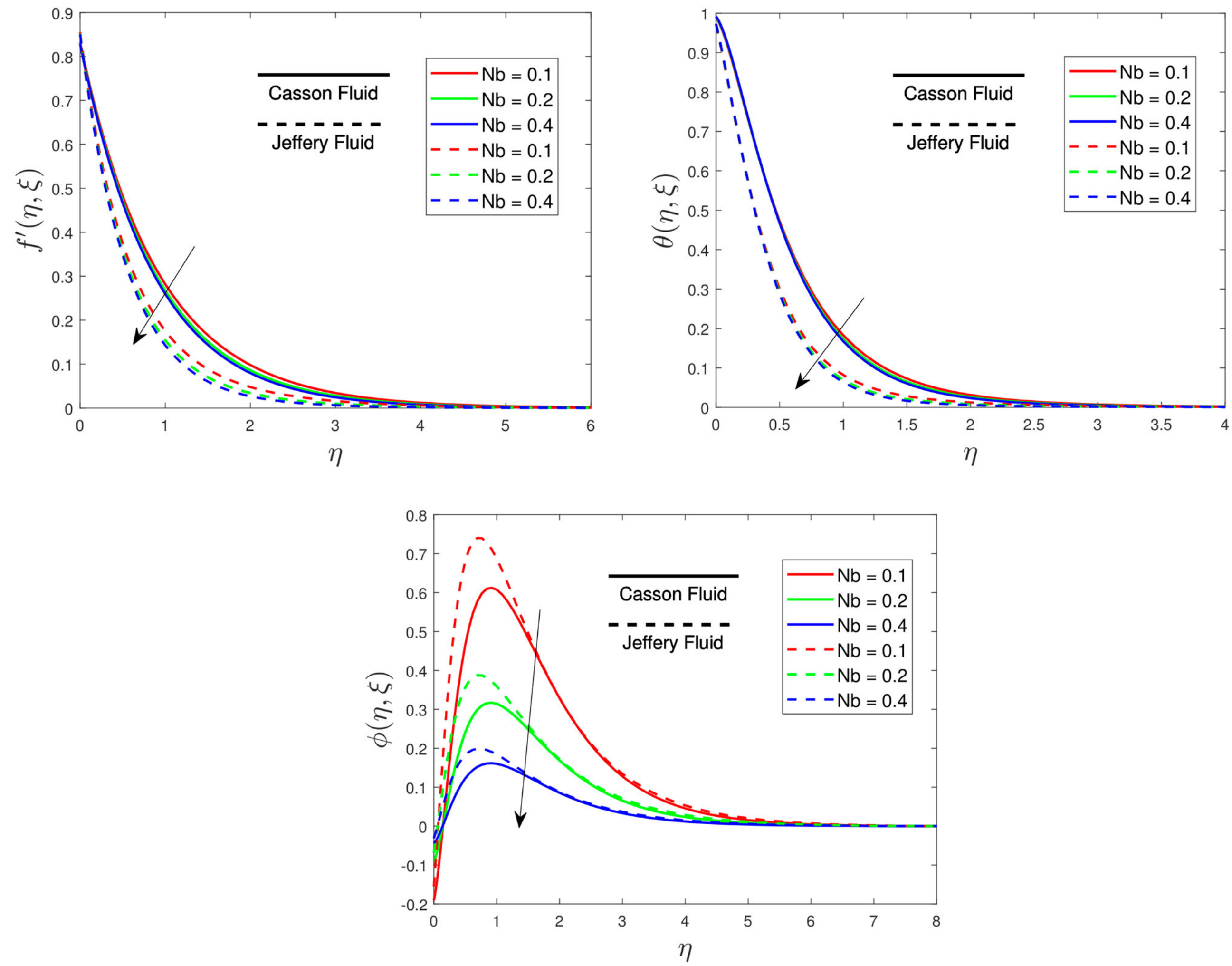

Figure 7. Brownian movement (Nb) influence on the flow profiles.

The behaviour of both fluids, subject to a parameter that characterises their non-Newtonian nature, is shown in Figure 9. The Casson parameter (β) represents the yield stress ratio to the fluid's viscoplasticity. This parameter determines how the Casson fluid behaves under applied stress. We note that increasing β indicates the fluid is more resistant to flow until a certain stress threshold is reached. The response of the Jeffrey fluid is strongly influenced by the interaction between its viscosity and relaxation term. As the parameter λ increases, the fluid viscosity rises, reducing flow rates. Slower flow rate leads to lesser heat transfer, thus less kinetic energy is generated, resulting in lower temperature distribution within the fluid. However, due to the reduced heat transfer and flow rate, fewer reactants are consumed, thereby enhancing the thickness of the concentration boundary layer.

Table 3 presents the effect of various thermophysical parameters on the engineering quantities of interest. As the fluid velocity becomes less sensitive to the temperature and concentration gradients of both fluids, the drag coefficient and heat transfer rate decrease. In contrast, the mass transfer coefficients for both fluids increase. However, as the kinetic energy to enthalpy ratio in both fluids decreases, the heat transfer rate increases, indicating enhanced thermal energy exchange. Conversely, both the drag force and the mass transfer coefficient decrease, suggesting reduced resistance to flow and lower rates of mass transfer across the fluid interface. This result implies that changes in the balance between kinetic energy and enthalpy significantly impact the overall transport properties of the system.

5. Conclusion

This study has shed light on the interplay between Casson and Jeffery nanofluid flows over an expanding surface without the need for independent simulations of each fluid's flow separately. This research provides a deeper understanding of the influence of common-cause effects on flow, heat, and species transfer mechanisms, as well as the behaviour of nanofluids under specific conditions, emphasising their impact on flow dynamics. The nanoparticles are mathematically modelled using Buongiorno's model. The model described the random movement of nanoparticles due to thermal agitation and response to concentration gradients, which significantly influence the diffusion and dispersion of the nanoparticles in the fluid, respectively. The fluids are

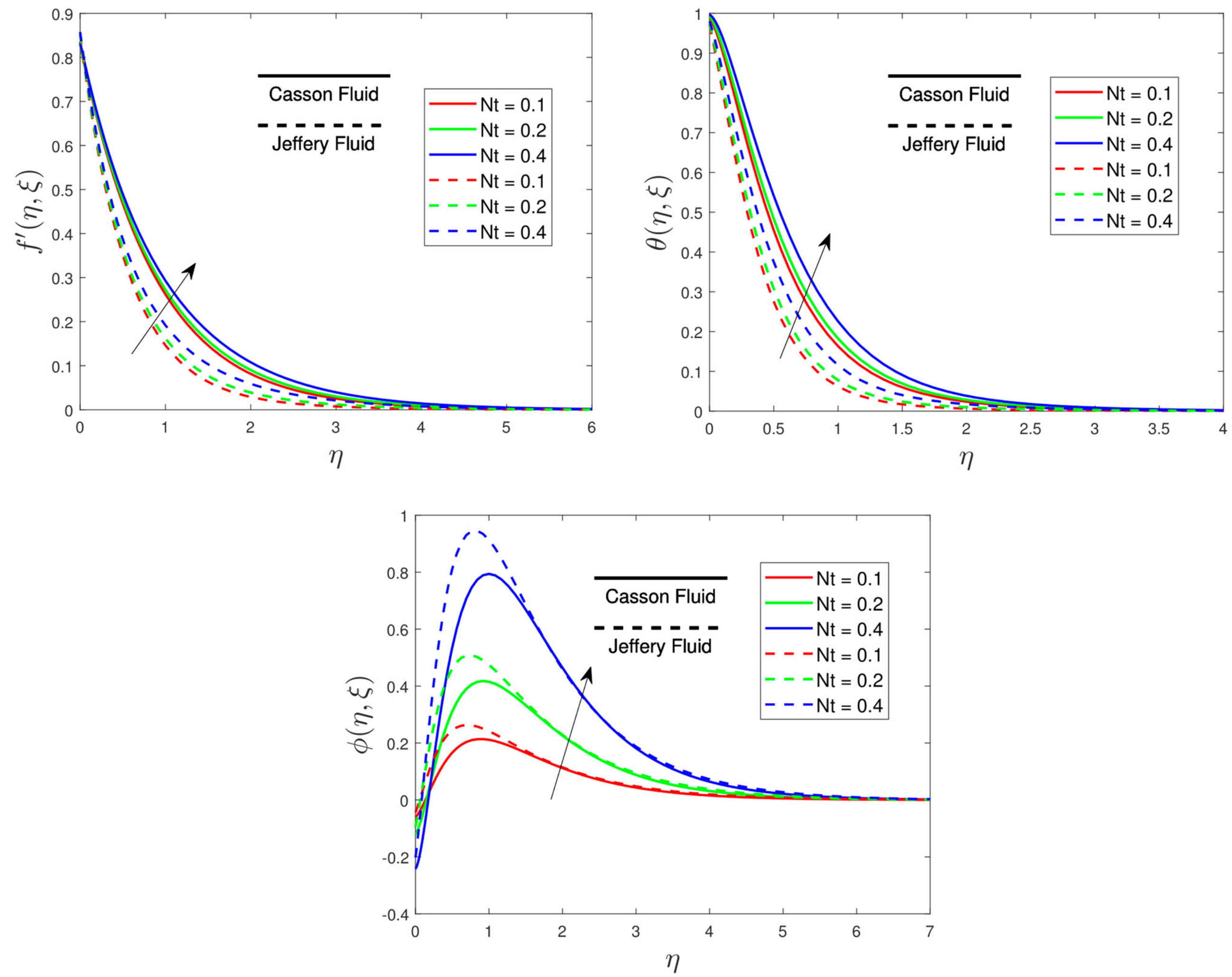

Figure 8. Thermophoresis ratio (Nt) influence on the flow profiles.

Table 3. Numerical values of drag coefficients ($Re^{\frac{1}{2}}Cf$), Nusselt number ($Re^{-\frac{1}{2}}Nu$) and Sherwood number ($Re^{-\frac{1}{2}}Sh$) using the value $f_w = 0.8$, $Nr = 0.5$, $\delta_1 = 0.1, M = 2.0$, $\Omega = 1.0$, $Nt = 0.15$, $\gamma_2 = 0.1, \gamma_2 = 0.1$, $\delta = 0.1$, $\delta_2 = 0.02$, $Kr = 0.05$, $E = 0.2$, $Nb = 0.2$, $n = 1.0$ and $\xi = 1.0$.

					Casson fluid ($De = \lambda = 0.0$)			Jeffrey fluid ($\beta \to \infty$)		
Pr	De	λ_2	λ_3	Ec	$Re^{\frac{1}{2}}Cf$	$Re^{-\frac{1}{2}}Nu$	$Re^{-\frac{1}{2}}Sh$	$Re^{\frac{1}{2}}Cf$	$Re^{-\frac{1}{2}}Nu$	$Re^{-\frac{1}{2}}Sh$
.2	0.01	0.2	0.2	0.5	−2.73596	3.26702	−0.92596	−2.03305	3.83888	−1.09105
.0	–	–	–	–	−2.73888	3.48863	−0.98983	−2.03625	4.11915	−1.17230
.0	–	–	–	–	−2.74193	3.75690	−1.06733	−2.03963	4.45862	−1.27101
.2	0.009	0.2	0.2	0.5	–	–	–	−2.03172	3.83950	−1.09123
-	0.010	–	–	–	–	–	–	−2.03305	3.83888	−1.09105
-	0.015	–	–	–	–	–	–	−2.03970	3.83578	−1.09016
.2	0.01	0.2	0.2	0.5	−2.73596	3.26702	−0.92597	−2.03305	3.83888	−1.09105
-	–	0.1	–	–	−2.80724	3.23283	−0.91612	−2.08669	3.80805	−1.08213
-	–	0.0	–	–	−2.87793	3.19812	−0.90614	−2.14007	3.77646	−1.07299
.2	0.01	0.2	0.2	0.5	−2.73596	3.26702	−0.92596	−2.03305	3.83888	−1.09105
-	–	–	0.1	–	−2.77140	3.22852	−0.91489	−2.07067	3.79059	−1.07708
-	–	–	0.0	–	−2.80782	3.18780	−0.90317	−2.11009	3.73776	−1.06180
.2	0.01	0.2	0.2	0.5	−2.73596	3.26702	−0.92596	−2.03305	3.83888	−1.09105
-	–	–	–	0.3	−2.75837	4.69909	−1.34113	−2.04541	5.03147	−1.43833
-	–	–	–	0.1	−2.78097	6.12537	−1.76049	−2.05790	6.22594	−1.79029

sensitive to thermal changes and chemical reactions, meaning their behaviour and properties are influenced by temperature variations and chemical interactions. After performing a non-similar analysis of the governing conservation equations, the physical system was reduced to a system of equations with two independent variables. A bivariate spectral-based method was used to approximate the solutions of the deterministic equations, allowing for the analysis of the problem under study. The findings revealed that the behaviour of Casson and Jeffrey fluids is consistent for all parameter variations, whether an

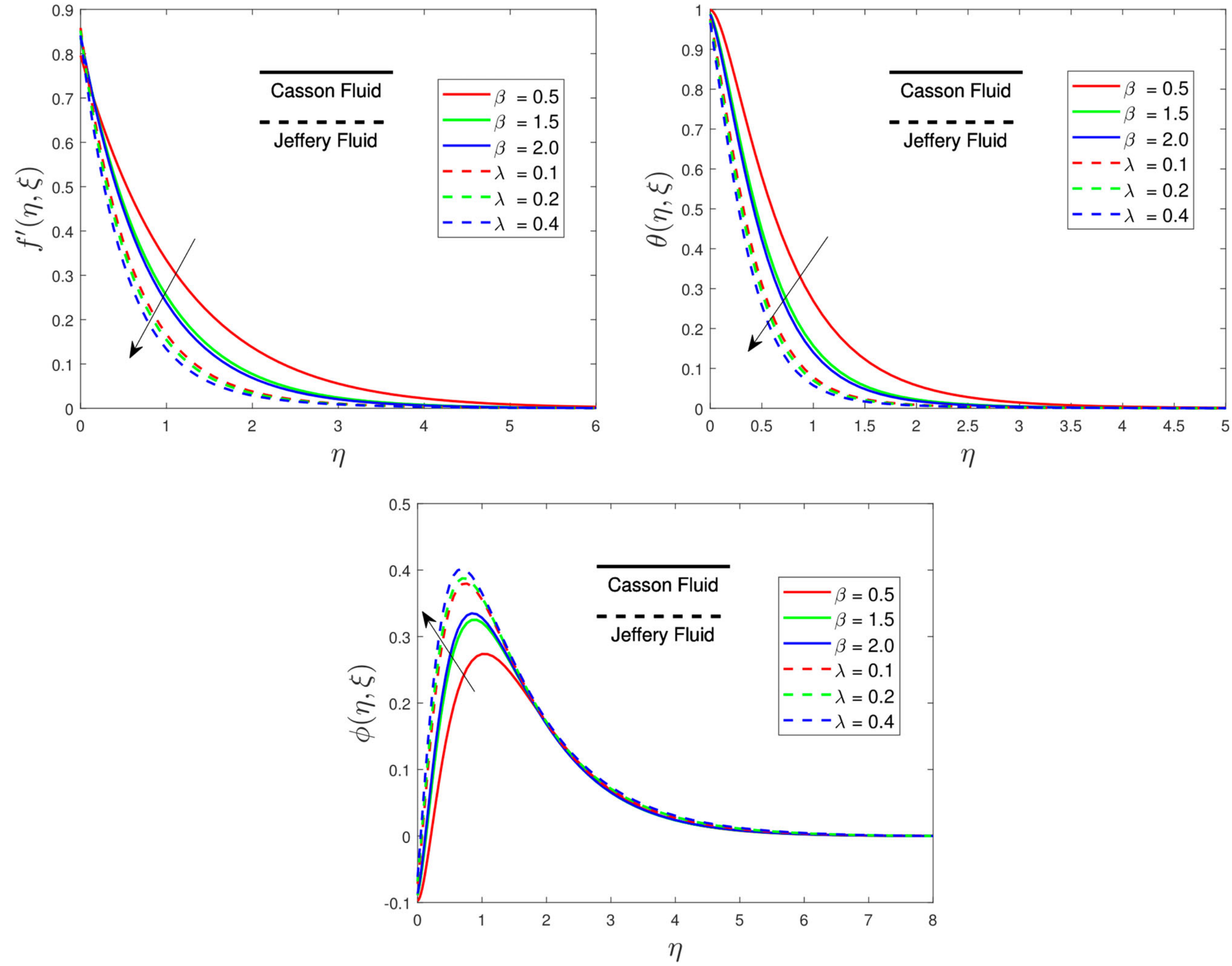

Figure 9. Casson (β) and Jeffrey fluids (λ) parameter influence on the flow profiles.

increase or decrease in a parameter enhances or reduces the fluid's response. The Casson fluid showed a greater tendency for flow and exhibited a higher temperature profile than the Jeffrey fluid. On the other hand, the Jeffrey fluid showed a more pronounced concentration profile, with stronger reaction characteristics, than the Casson fluid under similar conditions. Future research will explore the existence of dual solutions, perform stability analysis, and conduct a parametric study of the thermophysical effects under varying flow conditions.

Author contributions

CRediT: **Hammed Abiodun Ogunseye:** Conceptualization, Formal analysis, Investigation, Resources, Software, Writing – original draft, Writing – review & editing; **Yusuf Olatunji Tijani:** Conceptualization, Formal analysis, Investigation, Methodology, Software, Writing – original draft, Writing – review & editing; **Titilayo Morenike Agbaje:** Formal analysis, Methodology, Supervision, Writing – original draft, Writing – review & editing; **Shina Daniel Oloniiju:** Methodology, Software, Supervision, Writing – review & editing; **Olumuyiwa Otegbeye:** Formal analysis, Methodology, Supervision, Writing – review & editing

Disclosure statement

No potential conflict of interest was reported by the author(s).

ORCID

Hammed Abiodun Ogunseye http://orcid.org/0000-0003-3993-1585
Yusuf Olatunji Tijani http://orcid.org/0000-0002-9127-7173
Titilayo Morenike Agbaje http://orcid.org/0000-0002-8813-0955
Shina Daniel Oloniiju http://orcid.org/0000-0002-9794-8580
Olumuyiwa Otegbeye http://orcid.org/0000-0003-1321-9776

References

Akolade, M. T., T. A. Adeosun, and J. O. Olabode. 2021. "Influence of Thermophysical Features on MHD Squeezed Flow of Dissipative Casson Fluid with Chemical and Radiative Effects." *Journal of Applied and Computational Mechanics* 7 (4): 1999–2009.

Ashraf, M. W., J. A. Haider, H. A. Ghazwani, S. Ahmad, Z. Zheng, and S. Gul. 2024. "Force Convective Heat Transfer Simulation in a Rectangular Channel with Multiple Square Obstacles via Finite Element Method." *Modern Physics Letters B* 38 (29): 2450244. https://doi.org/10.1142/S0217984924502440

Canuto, C., M. Y. Hussaini, A. Quarteroni, and T. A. Zang. 2006. *Spectral Methods: Fundamentals in Single Domains*. Berlin: Springer-Verlag.

Dadhich, Y., R. Jain, A. R. Kaladgi, M. Alwetaishi, A. Afzal, and C. A. Saleel. 2021. "Thermally Radiated Jeffery Fluid Flow with Nanoparticles over a Surface of Varying Thickness in the Influence of Heat Source." *Case Studies in Thermal Engineering* 28:101549. https://doi.org/10.1016/j.csite.2021.101549

Das, M., R. Mahato, and R. Nandkeolyar. 2015. "Newtonian Heating Effect on Unsteady Hydromagnetic Casson Fluid Flow Past a Flat Plate with

Heat and Mass Transfer." *Alexandria Engineering Journal* 54 (4): 871–879. https://doi.org/10.1016/j.aej.2015.07.007

Goqo, S. *P*., S. D. Oloniiju, H. Mondal, *P*. Sibanda, and S. S. Motsa. 2018. "Entropy Generation in MHD Radiative Viscous Nanofluid Flow over a Porous Wedge Using the Bivariate Spectral Quasi-linearization Method." *Case Studies in Thermal Engineering* 12:774–788. https://doi.org/10.1016/j.csite.2018.10.005

Haider, J. A., S. Gul, and S. Nadeem. 2023. "Numerical Investigation of the Heat Transfer and Peristaltic Flow through a Asymmetric Channel Having Variable Viscosity and Electric Conductivity." *Scientia Iranica* 0 (0): 1–25. https://doi.org/10.24200/sci.2023.60404.6783

Hamid, A., M. Khan, and A. Hussain. 2020. "Performance of Heat Transfer in MHD Mixed Convection Flow Using Nanofluids in the Presence of Viscous Dissipation: Local non-similarity Solution." *Modern Physics Letters B* 34 (11): 2050101. https://doi.org/10.1142/S0217984920501018

Jan, A., M. Mushtaq, and M. Hussain. 2024. "Heat Transfer Enhancement of Forced Convection Magnetized Cross Model Ternary Hybrid Nanofluid Flow over a Stretching Cylinder: Non-similar Analysis." *International Journal of Heat and Fluid Flow* 106:109302. https://doi.org/10.1016/j.ijheatfluidflow.2024.109302

Khan, M., A. Rasheed, S. Ali, and Q. A. Azim. 2021. "A Novel Formulation of 3D Jeffery Fluid Flow near an Irregular Permeable Surface Having Chemical Reactive Species." *Advances in Mechanical Engineering* 13 (5): 1. https://doi.org/10.1177/16878140211013609

Khan, M., M. Waqas, T. Hayat, and A. Alsaedi. 2017. "A Modified Homogeneous-Heterogeneous Reactions for MHD Stagnation Flow with Viscous Dissipation and Joule Heating." *International Journal of Heat and Mass Transfer* 113:310–317. https://doi.org/10.1016/j.ijheatmasstransfer.2017.05.082

Kundu, *P*. K., I. M. Cohen, and D. R. Dowling. 2016. "Fluid Mechanics." *Academic Press* 6:1–921.

Kusiak, A., M. Li, and F. Tang. 2010. "Modeling and Optimization of HVAC Energy Consumption." *Applied Energy* 87 (10): 3092–3102. https://doi.org/10.1016/j.apenergy.2010.04.008

Kuznetsov, A., and D. Nield. 2014. "Natural Convective Boundary-Layer Flow of a Nanofluid Past a Vertical Plate: A Revised Model." *International Journal of Thermal Sciences* 77:126–129. https://doi.org/10.1016/j.ijthermalsci.2013.10.007

Lawal, M. O., Y. O. Tijani, S. O. Ajadi, and K. B. Kasali. 2023. "Simulation of the Laminar Thermal Boundary Layer Problem over a Flat Plate by Exploring the Local non-similarity Technique." *International Journal of Modelling and Simulation* 1:1–12.

Magagula, V. M., S. S. Motsa, and *P*. Sibanda. 2020. "On the Bivariate Spectral Quasilinearization Method for Nonlinear Boundary Layer Partial Differential Equations." In *Woodhead Publishing Series in Energy. Applications of Heat, Mass and Fluid Boundary Layers*, edited by R. O. Fagbenle, O. M. Amoo, S. Aliu, and A. Falana, 177–190. Sawston, Cambridge: Woodhead Publishing.

Magagula, V. M., S. S. Motsa, *P*. Sibanda, and *P*. G. Dlamini. 2016. "On a Bivariate Spectral Relaxation Method for Unsteady Magneto-Hydrodynamic Flow in Porous Media." *SpringerPlus* 5 (1): 1–15. https://doi.org/10.1186/s40064-016-2053-4

Mahesh, R., U. S. Mahabaleshwar, and F. Sofos. 2023. "Influence of Carbon Nanotube Suspensions on Casson Fluid Flow over a Permeable Shrinking Membrane: An Analytical Approach." *Scientific Reports* 13:3369. https://doi.org/10.1038/s41598-023-30482-6

Makanda, G., and S. Shaw. 2019. "Numerical Analysis of the Bivariate Local Linearization Method (BLLM) for Partial Differential Equations in Casson Fluid Flow." *WSEAS TRANSACTIONS on FLUID MECHANICS* 14:131–141.

Minkowycz, W. J., and *P*. Cheng. 1982. "Local non-similar Solutions for Free Convective Flow with Uniform Lateral Mass Flux in a Porous Medium." *Letters in Heat and Mass Transfer* 9 (3): 159–168. https://doi.org/10.1016/0094-4548(82)90054-6

Mkhatshwa, M. *P*., S. S. Motsa, and *P*. Sibanda. 2022. "Mhd Bioconvective Radiative Flow of Chemically Reactive Casson Nanofluid from a Vertical Surface with Variable Transport Properties." *International Journal of Ambient Energy* 43 (1): 3170–3188. https://doi.org/10.1080/01430750.2020.1818126

Mkhatshwa, M. *P*. 2024. "Nonlinear Convective Transport of Nanofluid over an Inclined Plate Situated in a Darcyâ€"Forchheimer Porous Medium with Viscous Dissipation and Varying Thermo-Physical Features." *International Journal of Ambient Energy* 25 (1): 2378945. https://doi.org/10.1080/01430750.2024.2378945

Motsa, S. S., and I. L. Animasaun. 2016. "Unsteady Boundary Layer Flow over a Vertical Surface due to Impulsive and Buoyancy in the Presence of Thermal-Diffusion and Diffusion-Thermo Using Bivariate Spectral Relaxation Method." *Journal of Applied Fluid Mechanics* 9 (5): 2605–2619.

Motsa, S. S. 2013. "A new Spectral Local Linearization Method for Nonlinear Boundary Layer Flow Problems." *Journal of Applied Mathematics* 2013 (1): 423628.

Motsa, S. 2015. "On the new Bivariate Local Linearisation Method for Solving Coupled Partial Differential Equations in Some Applications of Unsteady Fluid Flows with Heat and Mass Transfer." In *IntechOpen*, edited by M. Solecki, 1–15. London, UK: Mass Transfer: Advancement in Process Modelling, Woodhead Publishing.

Mukhopadhyay, S. 2013. "Slip Effects on MHD Boundary Layer Flow over an Exponentially Stretching Sheet with Suction/Blowing and Thermal Radiation." *Ain Shams Engineering Journal* 44: 485–491.

Neuzil, *P*., S. Giselbrecht, K. LÃnge, T. J. Huang, and A. Manz. 2012. "Revisiting lab-on-a-chip Technology for Drug Discovery." *Nature Reviews Drug Discovery* 11 (8): 620–632. https://doi.org/10.1038/nrd3799

Pantokratoras, A. 2019. "Four Usual Errors Made in Investigation of Boundary Layer Flows." *Powder Technology* 353:505–508. https://doi.org/10.1016/j.powtec.2019.05.060

Patil, *P*., S. Roy, and A. Chamkha. 2010. "Mixed Convection Flow over a Vertical Power-law Stretching Sheet." *International Journal of Numerical Methods for Heat and Fluid Flow* 20 (4): 445–458. https://doi.org/10.1108/09615531011035839

Qasim, M. 2013. "Heat and Mass Transfer in a Jeffrey Fluid over a Stretching Sheet with Heat Source/Sink." *Alexandria Engineering Journal* 52 (4): 571–575. https://doi.org/10.1016/j.aej.2013.08.004

RamReddy, C., and C. V. Rao. 2017. "Bivariate Pseudo-spectral Local Linearisation Method for Mixed Convective Flow over the Vertical Frustum of a Cone in a Nanofluid with Soret and Viscous Dissipation Effects." *Journal of Mechanics* 33 (5): 687–702. https://doi.org/10.1017/jmech.2017.63

Sandeep, N., and C. Sulochana. 2018. "Momentum and Heat Transfer Behaviour of Jeffrey, Maxwell and Oldroyd-b Nanofluids Past a Stretching Surface with non-uniform Heat Source/Sink." *Ain Shams Engineering Journal* 9 (4): 517–524. https://doi.org/10.1016/j.asej.2016.02.008

Schwab, K. 2016. The Fourth Industrial Revolution: What It Means, How to Respond. https://www.weforum.org/agenda/2016/01/the-fourth-industrial-revolution-What-It-means-and-How-to-respond/, 2015:2.

Shukla, N., *P*. Rana, S. Kuharat, and O. Anwar-BÃ©g. 2022. "Non-similar Radiative Bioconvection Nanofluid Flow under Oblique Magnetic Field with Entropy Generation." *Journal of Applied and Computational Mechanics* 8 (1): 206–218.

Siddiqui, A. M., A. A. Farooq, and M. A. Rana. 2015. "A Mathematical Model for the Flow of a Casson Fluid due to Metachronal Beating of Cilia in a Tube." *Scientific World Journal* 2015 (1): 487819. https://doi.org/10.1155/2015/487819

Sithole, H., H. Mondal, V. M. Magagula, *P*. Sibanda, and S. Motsa. 2019. "Bivariate Spectral Local Linearisation Method (Bsllm) for Unsteady MHD Micropolar-Nanofluids with Homogeneous' Heterogeneous Chemical Reactions over a Stretching Surface." *International Journal of Applied and Computational Mathematics* 5: 12. https://doi.org/10.1007/s40819–018–0593–8.

Sparrow, E. M., H. Quack, and C. J. Boerner. 1970. "Local Non-similarity Boundary Layer Solutions." *Aero and Astro Journal* 8:1936–1942.

Tijani, Y. O., A. T. Adeosun, H. A. Ogunseye, and H. Niranjan. 2024a. "Magnetic Dipole Dynamics on Reiner-Philippoff Boundary Layer Flow." *Numerical Heat Transfer, Part A: Applications* 85 (10): 1691–1705. https://doi.org/10.1080/10407782.2023.2209925

Tijani, Y. O., M. T. Akolade, O. Otegbeye, and A. Yusuf. 2024b. "Surface Dynamics on Jeffrey Nanofluid Flow with Coriolis Effect and Variable Darcy Regime." *ZAMM - Journal of Applied Mathematics and Mechanics / Zeitschrift Angewandte Mathematik und Mechanik* 104 (2): 152–160.

Tijani, Y. O. 2025. "Sensitivity and Numerical Simulation of Unsteady Reactive Hydromagnetic Eyring-Powell Flow in a non-horizontal Channel." *Multiscale and Multidisciplinary Modeling, Experiments and Design* 8 (305): 1–15.

Trefethen, L. N. 2000. *Spectral Methods in MATLAB*. Philadelphia, PA: SIAM.

Turkyilmazoglu, M. 2016. “Magnetic Field and Slip Effects on the Flow and Heat Transfer of Stagnation Point Jeffrey Fluid over Deformable Surfaces.” *Zeitschrift für Naturforschung a* 71 (6): 549–556. https://doi.org/10.1515/zna-2016-0047

Ullah, R., N. Israr Ur Rehmam, A. Hamid, S. Arooj, and W. A. Khan. 2024. “Heat and Mass Transport Aspect on Magnetised Jeffery Fluid Flow over a Stretching Cylinder with the Cattaneo-Christov Heat Flux Model.” *Molecular Physics* 122 (11): e2288701. https://doi.org/10.1080/00268976.2023.2288701

Wajihah, S. A., and D. S. Sankar. 2023. “A Review on non-newtonian Fluid Models for Multi-layered Blood Rheology in Constricted Arteries.” *Archive of Applied Mechanics* 93 (5): 1771–1796. https://doi.org/10.1007/s00419-023-02368-6

White, F. M. 2006. *Viscous Fluid Flow*. 3rd ed. New York: McGraw-Hill. 1:1–250.